Radboud Universiteit Nijmegen

An analysis of the energy reconstruction of Michel electrons at ProtoDUNE

Author:
Björk Johannes

Supervisor:
Dr. Frank Filthaut

December 2019

Abstract

In the analysis of Monte Carlo data of ProtoDUNE, problems are found related to the energy reconstruction software. This is especially problematic for using the data to find the polarization of cosmic muons and the influence of interactions of cosmic muons with the argon atoms in the Liquid Argon Time Projection Chamber (LArTPC) at ProtoDUNE on which the Monte Carlo simulations are based.

Previous studies mention the presence of bremsstrahlung to be the main contributing factor of the faulty reconstruction. In this thesis, other possible factors are discussed as well as the presence of radiative energy losses, which are not taken into account in the reconstruction process. Through various Monte Carlo simulations, the differences between the true data and the reconstructed data are discussed and with those results, the Monte Carlo simulations are improved until a simulation is carried out that matches the actual situation the best. From this final simulation, another possible cause of the reconstruction problems is found. Charge deposited by one of the decay products of the cosmic muon, the Michel electron, might have been included into the muon track rather than the electron track. Other causes that are studied, like the influence of the directions of the particles with respect to each other and with respect to the detector, do not provide clear prove of their relation to the reconstruction problems.

It is likely that there are other causes than merely the exclusion of radiative energy losses, which need to be studied more closely to provide actual numerical values of those influences. Further studies could provide actual numerical values of these influences and make better reconstructions possible. When this is done, only then something can be said about the polarization of cosmic muons at ProtoDUNE.

Contents

1 Introduction

The original goal for the study described in this thesis, was to find the polarization of cosmic muons at ProtoDUNE, the prototype of the Deep Underground Neutrino Experiment (DUNE), which will be realised at Fermilab, Chicago, in 2026. At DUNE the ultimate goal is to obtain a greater understanding of the origin of matter, the unification of forces and black hole formation. Before the massive detectors are build in Chicago, they ought to be tested at a smaller scale. This was done at CERN. In this thesis simulations of ProtoDUNE are used as well as some actual data from ProtoDUNE. At ProtoDUNE, muons will travel through a tank filled with liquid argon, where they lose their energy and decay into an electron and two neutrinos. Theoretically, the polarization of the muons for this particular decay can be expressed through angular momentum conservation and the helicity of the particles. From that point of view, the polarization should be within a close proximity of $+1$ for negatively charged muons and within a close proximity of -1 for positively charged muons. However, the decay into an electron happens when the particle is at rest, after interacting with many argon atoms. Those interactions could have an influence on the polarization, which could approach zero as a result. Before this hypothesis can be tested, two variables were needed. The energy of the electron that was the decay product of the muon and the cosmic angle, the angle between the muon direction at the end of its track and the electron direction at the beginning of its track. With the simulated data, those variables can be reconstructed. During this study it became clear that the reconstruction is biased and could not be used for the original goal without a correction. It also became clear that a correction could only be made if the cause of the biased reconstruction is numerically analyzed. This appeared to be not within the reach of a bachelor's thesis. However, the results of the simulations and reconstruction process are analyzed and some probable causes of the biased reconstruction are discussed.

My motivation for this study was the performing of data analysis. Experimental high energy physics and in particular data analysis is not a general subject taught at the Radboud University on bachelor level. In order to make the right choice of master specialisation, the bachelor thesis seemed to be a prefect opportunity to delve into this aspect of physics. This combination of theoretical with experimental physics proved to be a perfect fit with my interests. I would have preferred to be able to carry out the actual fit to find the polarization of the muon, which seemed to be too far a stretch. Nevertheless, I have learned a lot from this study on data analysis and the performing of research in general.

2 Theory

2.1 Cosmic muons

Cosmic muons are particles that are created in the atmosphere via cosmic showers. They can be the product of the decay of pions. For a pion, the decay into a muon is its dominant decay and is given below. A pion is a meson consisting of a quark and an anti-quark, π^+ consists of $u\bar{d}$, π^- consists of $\bar{u}d$ and π^0 consists of either $\bar{u}u$ or $\bar{d}d$. For muons, only the charged pions are of importance. The operating force in the following decay is the weak interaction ($W^\pm$).

$$\begin{aligned} \pi^+ &\to \mu^+ + \nu_\mu \\ \pi^- &\to \mu^- + \bar{\nu_\mu} \end{aligned} \tag{1}$$

A muon can also be the decay product of kaons. The relevant kaon decay for cosmic muons are mesons consisting of up and strange quarks: $u\bar{s}$ and $s\bar{u}$, for K^+ and K^- respectively. Like the pion, we also have $K^\pm$ decaying into a muon and a neutrino.

$$\begin{aligned} K^+ &\to \mu^+ + \nu_\mu \\ K^- &\to \mu^- + \bar{\nu_\mu} \end{aligned} \tag{2}$$

These decays are the most dominant of their kind, in which the produced muons take on average 79% and 52% of the energy of the $\pi^\pm$ and $K^\pm$, respectively.[1]

Muons arrive at sea level with an average flux of about 1 muon per square centimeter per minute. This is about half of the typical total natural radiation background.[2] ProtoDUNE at CERN first measured with a muon beam. At this time, however, the beam is not operating. To still be able to acquire data, they have analyzed cosmic muons instead, since there are so many of them.

2.1.1 Polarization

The polarization of the muon depends on the spin of all muons within a certain, chosen, range. Muons with negative charge, originating from the pion decay, have a left-handed fixed chirality and a mostly right-handed helicity. The helicity is defined by the projection of the spin onto the momentum of the muon. The chirality for massless particles is the same as the helicity for massless particles. For massive particles chirality is fixed, like a quantum number, while helicity can change. The negatively charged muon is right-handed to conserve angular momentum since the anti-neutrino *must* be right-handed because they are nearly massless.[3] This also means that a muon with positive spin aligned with the flight direction would be right-handed and a muon with negative spin in the opposite of the flight direction would be left-handed.[4]

In the figure 1, this is schematically displayed. The white arrows indicate the flight direction and the black arrows indicate the spin direction. The red arrow is the boost direction of the pion, pointed towards earth. Here it is shown that μ^+ has its spin in the opposite direction as its momentum, hence, the μ^+ is *left-handed*. For the μ^-, the spin points in the same direction as its momentum. The μ^- is *right-handed*.

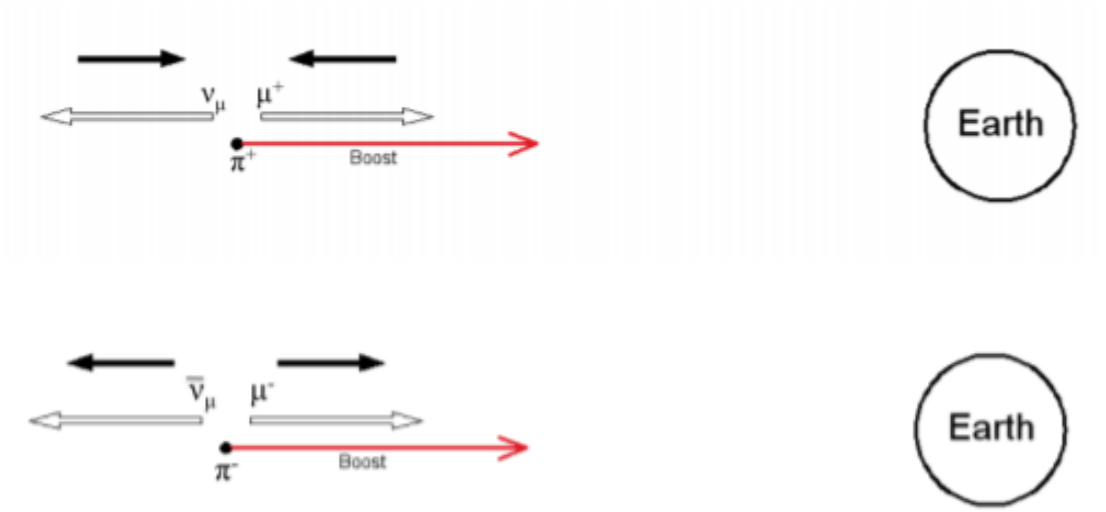

Figure 1: The decayed pion releases a muon in the boost direction or in the opposite direction. We only look at muons moving towards earth, both positively charged as negatively charged.[5]

For extremely high energetic pions, it is possible to decay into a left-handed muon and right-handed anti-muon. This can only be the case if the neutrino, which always has fixed helicity, is emitted in the same direction as the muon. Since the energy of the pion drops with intensity, lesser pions are extremely high energetic, which results in a net helicity of right-handed muons and left-handed anti-muons.[5]

The polarization is defined by the projection of the spin onto the quantization axis. For the polarization we can choose the quantization axis. For simplicity, we want the polarization axis to align with the direction of the muon. In this case the polarization is simply the net helicity. The polarization is defined as

$$P = \frac{N(\uparrow) - N(\downarrow)}{N(\uparrow) + N(\downarrow)} \tag{3}$$

where $N(\uparrow)$ is the number of right-handed (anti-)muons and $N(\downarrow)$ the number of left-handed (anti-)muons. For a net right-handed helicity, an abundance right-handed (anti-)muons, we expect $N(\uparrow)$ to be greater than $N(\downarrow)$ which results in a positive net polarization. For a net left-handed helicity we expect $N(\downarrow)$ to be greater. Since we expect almost all negatively charged muons to be right-handed and almost all positive muons to be left-handed, the polarization for muons should be within a close proximity of +1, while for anti-muons this should be within a close proximity of -1.[6]

2.1.2 Muon decay

The dominant muon decay is when the muon ($\mu^\pm$) decays into an electron ($e^\pm$) and two neutrinos ($\nu_{e,\mu}$). The Feynmann diagram of such a decay is seen in figure 2.

$$\begin{aligned} \mu^- &\rightarrow e^- + \bar{\nu_e} + \nu_\mu \\ \mu^+ &\rightarrow e^+ + \nu_e + \bar{\nu_\mu} \end{aligned} \tag{4}$$

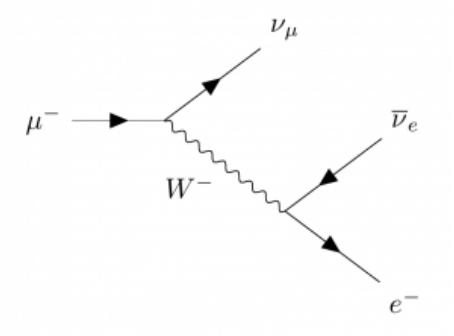

Figure 2: Negatively charged muon decay to a Michel electron.[7]

When the muon decays at rest is also called the Michel decay and the electron is called the Michel electron. The data that is used for this thesis contains both positively charged muons as negatively charged muons, without any means of telling the difference between the two. The muon has an average lifetime τ in vacuum of $(2.196\,981\,1 \pm 0.000\,002\,2)$ µs, but the lifetime differs slightly for a muon or anti-muon.[8]

The decay width of a particular particle decay is defined as Γ and scales with $\frac{1}{\tau}$, in this case, the lifetime of the muon. The differential decay width is given below and is also called the decay distribution. The $\pm$ relates to $\mu^\pm$ being the incmoing particle.

$$\begin{gathered} \frac{\partial^2\Gamma}{\partial x \partial cos(\alpha)} \approx x^2 \cdot (3(1-x) + \frac{2\rho}{3}(4x-3) + 3\eta x_0(1-x)/x \pm P_\mu \xi cos(\alpha)(1-x+\frac{2\delta}{3}(4x-3)) \\ x = \frac{2E_e}{m_\mu} \end{gathered} \tag{5}$$

The differential decay width depends on $cos(\alpha)$, which is defined as the angle between the stopping muon and the Michel electron formed by its decay, and will be called cosmic angle from this point forward. The reduced energy of the electron x is the energy scaled with the rest mass of the muon m_μ, which is the energy of the muon just before it decays into the electron. $x_0 = m_e/W_{e\mu}$, where $W_{e\mu}$ is the maximum electron energy and equals roughly half of the muon mass, which means that $x_0 = 9.67 \times 10^{-3}$. It also depends on the polarization vector $\overrightarrow{P_\mu}$, with length $P_\mu = |\overrightarrow{P_\mu}|$, and the Michel parameters. The Michel parameters for the Standard Model coupling are $\rho = \xi\delta = 3/4$, $\xi = 1$ and $\eta = 0$[8]. This results in a differential decay rate of

$$\frac{\partial^2\Gamma}{\partial x \partial cos(\alpha)} = \frac{G_F^2 m_\mu^5}{192\pi^3}(3 - 2x \pm P_\mu cos(\alpha)(2x-1))x^2, \tag{6}$$

which is independent of x_0. The differential decay rate in formula 5 can give information about the probability that a $\mu^\pm$ decays into an $e^\pm$ with energy $x+dx$ within an angle $cos(\alpha)+dcos(\alpha)$. We expect the cosmic angle $cos(\alpha)$ to be within a close proximity of $+1$, due to chirality conservation, thus expecting the Michel electron travels in the same direction as the muon before it decayed.

2.2 Energy loss in matter

Particles can be detected only through their interaction with matter. There are several ways that particles can lose energy in matter. The most relevant ones, for charged particles, are ionization and excitation. However, for relativistic particles, or high energetic particles, bremsstrahlung must also be taken into account. Other types of energy loss that appear in electromagnetic processes that are relevant are Coulomb scattering, Cherenkov light, scintillation light, pair production (for e.g.) photons and nuclear interactions.[9] Neutral particles, e.g. photons, can be detected by photon detectors or by the charged particles that are created by the photons.

Bremsstrahlung is the process where charged particles interact with the electromagnetic field of the atomic nuclei. The charged particle gets deflected by the nucleus and loses kinetic energy through a photon. Ionization is the process where charged particles travelling through matter lose energy through excitation and ionization of, in this experiment, argon atoms. The energy loss is described in energy per unit of column depth (MeV/(g/cm^2)). Excitation and ionization losses are described with the same equation, the Bethe-formula, that will be described later. For excitation, electrons are not freed but fall back to their ground state, releasing a photon. To trace back the particle to their moment of origin, scintillation light can be of importance. Scintillation light consists of photons that are emitted in the excitation process and have a typical peak at 128 nm and a decay time of 6.16 ns for liquid argon.[10],[11] Since they travel with the speed of light and can be matched with the correct event, this is a good indication to measure the time of decay t_0.

2.2.1 Muons

For a muon, the energy loss in matter is described rather well with the Bethe-formula. This equation describes the energy loss (mass stopping power) by ionization and excitation. The formula can be written as

$$\begin{aligned} \left\langle -\frac{dE}{dx} \right\rangle &= Kz^2 \frac{Z}{A} \frac{1}{\beta^2} \left\{ \frac{1}{2} \ln \frac{2m_e c^2 \beta^2 \gamma^2 W_{max}}{I^2} - \beta^2 - \frac{\delta(\beta\gamma)}{2} \right\} \\ W_{max} &= \frac{2m_e c^2 \beta^2 \gamma^2}{1 + 2m_e/M\gamma + (m_e/M)^2}, \end{aligned} \tag{7}$$

where $K = 4\pi N_A r_e^2 m_e c^2 =$ is a constant, depending on the constant of Avogadro N_A, the average electron radius r_e, the rest mass of electrons m_e and the speed of light c. z is the charge of the incoming particle, Z is the atomic charge number of the material, A is the atomic mass number of the material, $\beta = \frac{v}{c}$ is the velocity of the electron, γ is the Lorentz factor, and I is the mean excitation energy. I can be approximated by $I = 16Z^{0.9}$eV for $Z > 1$.[12] W_{max} is the maximum amount of kinetic energy transferred to an electron in a single collision. Here, M is the mass of the incident particle.[13] The formula has units MeV/(g/cm^2) and dx has units g cm^{-2} since this is the area density unit and can be described as

$$dx = \rho ds, \tag{8}$$

where ρ is the density of the material in g cm^{-3} and ds a length in cm. For dense media there is a reduction of logarithmic rise, the density effect. $\delta(\beta\gamma)$ is the density effect correction factor for ionization energy loss. At very high energies the density effect is written as

$$\frac{\delta(\beta\gamma)}{2} \to \ln(\hbar\omega_p/I) + \ln(\beta\gamma) - 1/2, \tag{9}$$

where $\hbar\omega_p$ is the plasma energy. The density correction is parameterized by Sternheimer.[14] The Sternheimer parameterization leaves us with

$$\delta(\beta\gamma) = 2\ln(\beta\gamma) + C, \tag{10}$$

where C is the correction factor depending on the material that particles are passing through. Depending on the momenta of the particles, other parameters are added to give the best fit to recent calculations. In figure 3, the contribution of the density correction is shown. The green dotted line shows us the mass stopping power without the density effect in consideration, the red dotted line shows us the mass stopping power with the density effect taken into account. We can see that for higher momenta, the density effect becomes more important. For muons in liquid argon there is a figure similar to figure 3, but less descriptive. This figure can be found in section E.[15]

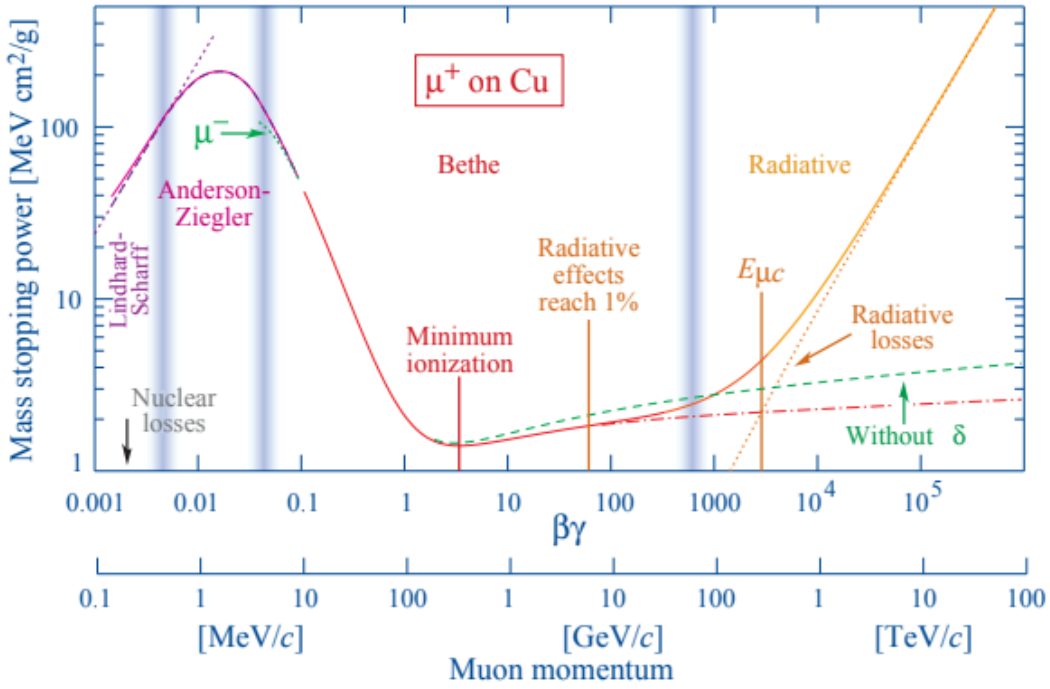

Figure 3: Mass stopping power for positive muons in copper as a function of $\beta\gamma = \frac{p}{Mc}$. The solid line indicates the total stopping power. The curve in the ionization region is described by the Bethe formula(7).[13]

The mass stopping power described by the Bethe-formula is the expected value of energy loss, or the mean value. The most probable value differs slightly and can be described by a Landau function depending on λ, where λ is defined as the deviation from the most probable energy loss (formula 11).

$$\begin{aligned} L(\lambda) &= \frac{1}{\sqrt{2\pi}} \exp\left[-\frac{1}{2}(\lambda + e^{-\lambda})\right] \\ \lambda &= \frac{\Delta E - \Delta E^{mp}}{\xi} \\ \xi &= \frac{K}{2}\langle\frac{Z}{A}\rangle z^2 \frac{x}{\beta^2} \end{aligned} \tag{11}$$

Here, ΔE is the actual value of energy loss in a layer of thickness x, while ΔE^{mp} is the most probable value. Experimentally, the energy-loss distribution is frequently found to be broader than represented by the Landau distribution.[12] The average value of the Landau distribution can be found with the Bethe equation. From the shape of the distribution it is expected that the Bethe value and the most probable value differ. An example of the Landau distribution for 10 MeV muons in liquid argon is shown in figure 4.[15]

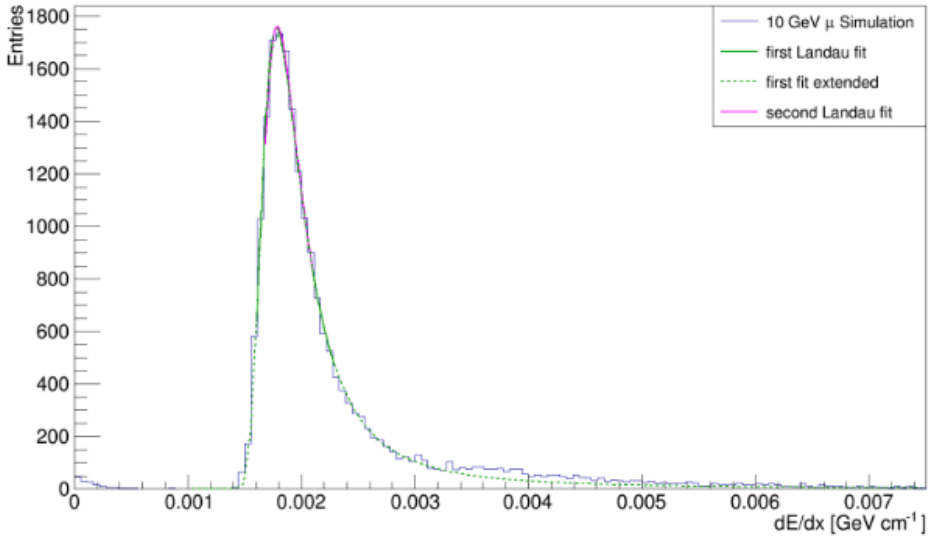

Figure 4: The Landau distribution of 10 MeV μ energy loss in the DUNE Far Detector simulated by K. Ingles.[15]

The most probable energy loss can be found and is described as

$$\Delta E^{mp} = \xi \left[\ln \frac{2m_e c^2 \beta^2 \gamma^2}{I} + \ln \frac{\xi}{I} + j - \beta^2 - \delta(\beta\gamma) \right], \tag{12}$$

where the most recent value of j equals $j = 0.200$.[16]

In high energy regions ($\beta\gamma \approx 100\,\text{GeV}$) equation 12 behaves like

$$\Delta E^{mp} \to \xi \left[\ln \frac{2m_e c^2 \xi}{(\hbar\omega_p)^2} + j \right], \tag{13}$$

which is what Landau expected.[17]

There are also other processes contributing to energy loss, however, for the ProtoDUNE experiment, those are of lesser importance, but will still be taken into account with the following equation.

$$\left\langle -\frac{dE}{dx} \right\rangle = a(E) + b(E)E \tag{14}$$

Here, $a(E)$ is described in equation 7 and $b(E)$ takes into account the other means of energy loss. $b(E)$ can therefore be split into three pieces.

$$b = b_{brems} + b_{pair} + b_{nucl} \tag{15}$$

b_i is the contribution of brehmsstrahlung, direct paired production and nuclear interactions, respectively, on the total energy loss. Pair production happens when a photon produces an electron/positron pair. The combination of brehmsstrahulung and pair production leads to a cascade, which runs until the produced particles are of a sufficiently low energy. The solid line in figure 3 is the total energy loss, taken into account the radiative energy losses of b_i. As we would expect, in the radiative region these contributions are considerably higher. In the figure there is also a contribution of δ-rays. δ-rays can be seen as electrons that contribute to a secondary ionization. Which means that ionized electrons with high energies can cause ionization themselves. This effect will not be taken into account in the reconstruction phase.

In conclusion, when every factor is taken into account, the mean energy loss is $dE/dx_{mean} = 2.1173\,\mathrm{MeV\,cm^{-1}}$ and the most probable energy loss is $dE/dx_{MPV} = 1.6339\,\mathrm{MeV\,cm^{-1}}$. In the Bethe-formula, the W-value for ionization $W_i = (23.6 \pm 0.3)\,\mathrm{MeV}$ is used.[11]

2.2.2 Electrons

For electrons the stopping power differs slightly. The Bethe function described "heavy" particles, which means, particles heavier than electrons. For electrons ionizing other electrons it is not possible to distinguish them, since their masses are equal. However, it can be described by energies, rather then masses, of incident and outgoing electrons. They are described by the Möller cross section. In the following equation $z = 1$ for electrons.

$$\left\langle -\frac{dE}{dx} \right\rangle = \frac{1}{2} K \frac{Z}{A} \frac{1}{\beta^2} \left\{ \frac{1}{2} \ln \frac{2 m_e c^2 \beta^2 \gamma^2 W_{max}}{I^2} + (1 - \beta^2) - \frac{2\gamma - 1}{\gamma^2} \ln 2 + \frac{1}{8} \left(\frac{\gamma - 1}{\gamma} \right)^2 - \delta \right\}$$

$$W_{max} = \frac{1}{g} m_e c^2 (\gamma - 1) \tag{16}$$

Here g is a factor depending on the type of scattering. For electron-electron scattering, this factor equals 2 since the particles are indistinguishable. For proton-electron scattering, this factor disappears.[13] Comparing the logarithmic term with the Bethe formula for "heavy" particles, one finds that they only differ by a factor $\ln 2$.

For high energy electrons, e.g. the Michel electron, bremsstrahlung is an important contribution to energy loss. The electron loses energy by bremsstrahlung at a rate nearly proportional to its own energy, while the ionization energy loss rate is only proportional to the logarithm of the electron energy. The critical energy (also seen in figure 3) is defined as the energy where ionization energy loss and radiative energy losses are equal. The critical energy in liquid argon is 30.5 MeV.[11] Energy loss through bremsstrahlung is described with the formula below. Here, α is the fine structure constant.[12]

$$-\frac{dE}{dx} \approx 4 \alpha N_A \frac{Z^2}{A} r_e^2 E \ln \frac{183}{Z^{1/3}} \tag{17}$$

2.2.3 Energy spectrum

For the data analysis later on, the energy of the electron is needed. Another important feature of the data reconstruction is the muon stopping point. One way to identify the muon stopping point in the upcoming experiment is the Bragg-peak. The muon has an energy stopping power as described in the previous sections. The Bragg-curve plots the muon stopping power during its travel through matter. A peak is observed where the muon quickly loses the remaining of its energy right before it comes to a rest and decays, which can be detected and is shown in section 3.2. The peak occurs because the cross-section increases when particles loses energy. This peak is also the only indication there is to make sure the muon was at rest, or close to being at rest. In the experiment only muons that are at rest will be looked at, so the Bragg-peak is also a selection requirement.

For the decay distribution of the muon to the electron there is a steep cut-off at an electron energy of about 53 MeV. The decay rate $\frac{d\Gamma}{dE}$ is described by equation 18 and is derived in the appendix, section A.

$$\frac{\partial\Gamma}{\partial x} = \frac{G_F^2 m_\mu^5}{192\pi^3}(6x^2 - 4x^3) \tag{18}$$

$\frac{d\Gamma}{dE}$ has a peak at the previously mentioned value and drops almost vertically at this point. The information that can be gained here is that the most probable energy of the electron will be 53 MeV, which is about the same as half of the muon mass. The electron energy can theoretically never be greater than E_{max}. Equation 18 is cut off at this point. The maximum possible energy is given below. Note that this is the total energy of the electron, while the figure below portrays the reduced kinetic energy as defined in equation 4.

$$E_{max} = \frac{m_\mu^2 + m_e^2}{2m_\mu} \tag{19}$$

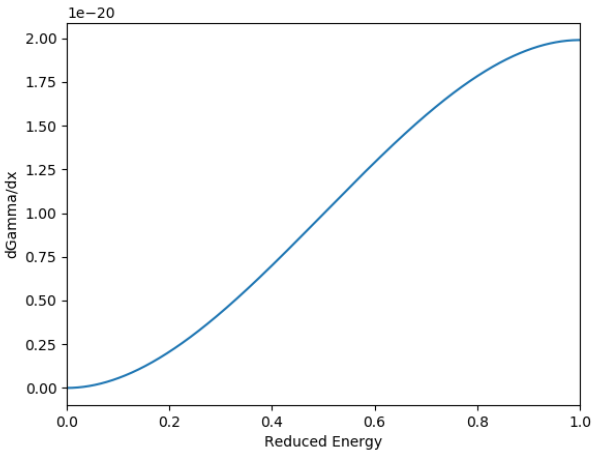

Figure 5: In this figure the expected decay curve, through integration of the differential decay over the cosmic angle, is shown. This curve is described by equation 18. It is cut off at a reduced energy of $x = 1$, the bounds of the theoretical value for the electron energy.

3 ProtoDUNE

The ProtoDUNE experiment is of uttermost importance to the future DUNE experiment. Here the detectors are tested, calibrated and, if necessary, altered. Whereas DUNE will consist of two neutrino detectors with a 1,300 kilometer distance between them, the ProtoDUNE experiment consists of two seperate detectors. A single phase (SP) and dual phase (DP) detector. The detectors in both experiments are Liquid Argon Time Projection Chambers (LArTPC), the SP-LArTPC at ProtoDUNE is 550 cubic meter, 90 times smaller than the detector planned for DUNE. The SP-detector has an effective mass of 770 tons of liquid argon.[18],[19] In this LArTPC cosmic muons are measured with a single-phase, multi-wire chamber. The data is then used to reconstruct the trajectory of the stopping muon and the energy of the corresponding emitted Michel electron.

3.1 Liquid Argon Time Projection Chamber

The two properties that can be measured in the LArTPC are light and charge. While photon detectors can measure scintillation light, the wires in the anode plane can measure charge. The set-up consists of two anode wire planes and a cathode plane, a field cage surrounding the planes and responsible for the electric field, a high voltage power supply, read-out electronics, a photon detection system (PDS), a data acquisition system, a cryostat, a purification system, and a detector control system.

The TPC has two anode planes at either side of the tank and one cathode plane in the middle of the chamber. The drift electric field is pointed towards the cathode plane, which makes negatively charged particles move towards the anode planes and positively charged particles move to the cathode plane. The anode is close to being grounded and the cathode has a voltage of $\approx -180\,\mathrm{kV}$ needed to produce a $500\,\mathrm{V\,cm^{-1}}$ drift electric field towards the anode. This corresponds effectively to a drift velocity of $0.165\,\mathrm{cm\,\mu s^{-1}}$[11] for the ionized electrons.

The anode planes consist of three separate wire planes stacked together, each of which has a different orientation. The first two wire planes are the induction planes and the last wire plane is the collection plane. The induction wire planes are orientated with an angle of 37.5°with respect to the vertical axis, to make sure each induction wire crosses a collection wire only once. The induction plane wires only give an induced electric signal. The charge then builds up in the collection wire plane when the wires "collect" the electrons, which produce the total signal.[19] In figure 6 the induction wire planes are green and pink, while the collection wire plane is blue. The cathode plane is made up of six cathode plane assembly columns and is designed to uphold the electric field. Each column consists of three modules stacked vertically, which makes the total number of modules 18 and the dimensions $7\,\mathrm{m} \times 6\,\mathrm{m}$.

To ionize an atom 23.6 eV is needed per electron-ion pair. Since the energy loss of the muon has a minimum of $2.12\,\mathrm{MeV\,cm^{-1}}$[11], every centimeter 9×10^4 electron-ion pairs are produced. The wire spacing is 4.7 mm, which results in a total of 42×10^3 electron-ion pairs per wire. Due to recombination, about half of the electrons will be absorbed by the ions again. This still leaves thousands of electrons left per wire. Therefore, the induced current spikes will exist of thousands of electrons. The induced current spikes on different wires will have a fraction of time between them which is used to reconstruct the trajectories. The build up charge in the collection plane is the output signal of the detector. This process is shown in figure 7 and elaborated on in the next section, section 3.2.

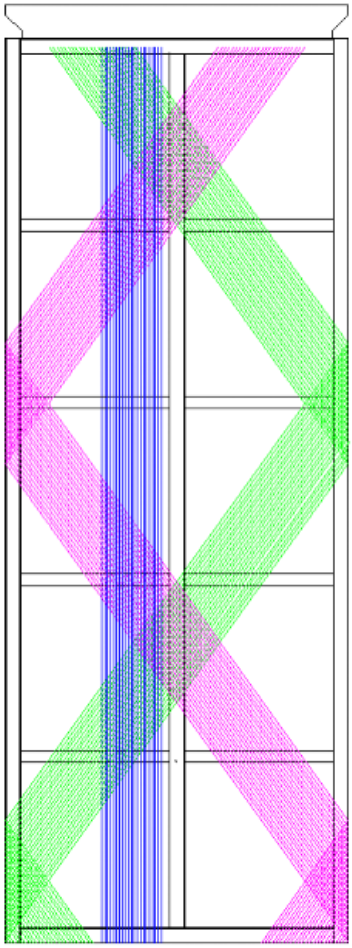

Figure 6: The layout of the anode wire plane where the induction planes are green and pink and the collection plane is blue.[19]

The photon detection system measures scintillation light and is used to obtain additional event information from the photons produced by particles travelling through the detector. Within the detector, only 19.5 eV[11] is needed to produce a photon. With an electric field such as that of the LArTPC, a typical particle generates an average of 20,000 photons per deposited MeV[19]. About 1/4 of the photons have a lifetime of 6 ns, while the rest of the photons yield a much larger lifetime of 1100-1600 ns. The photon detection systems detects both cases and the generated photons have a strong peak at 128 nm with an absorption length of >200 cm. All of this results in a relatively large light output and therefore a good method of determining t_0 when this is unknown (for interactions other than by beam particles) and can also be used for triggering the non-beam events.

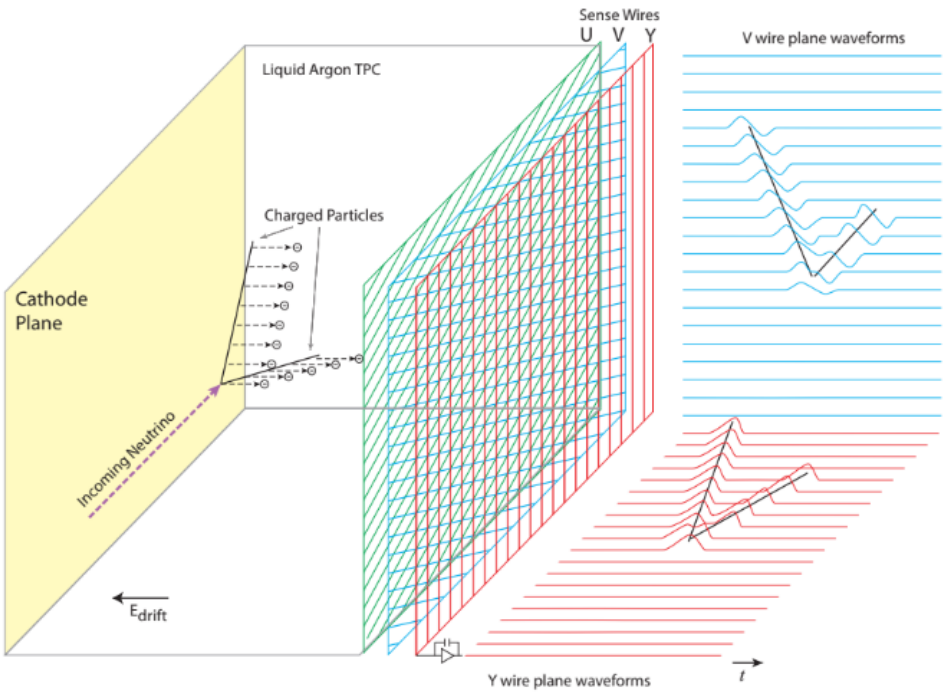

Figure 7: The LArTPC where the track of a particle is shown. In this set-up the induction wire planes are indicated by the letters U and V, while the collection wire plane has the letter Y. [20]

3.2 Data Reconstruction

In figure 7 one can see an incoming neutrino which decays into charged particles. The charged particles will ionize the liquid argon atoms and the freed electrons move towards the anode plane. The induction wires are used to determine the coordinates (y,z) of the particles by matching two intersecting wires on the different planes with coincident hits. We can see the direction of the time t, which gives us an indication of the x coordinate of the particles. In figure 28 in appendix E there is an example of multiple decay products where the signals overlap. The only type of information that is given is the charge signal from the wire planes. With this information there are numerous other properties that can be derived. The software that is used to reconstruct the Michel electron and the muon track is called LArSoft, a C++ based tool for simulation, reconstruction and data analysis for LArTPCs. There are three different approaches to reconstructing data, the one used here is called Pandora. The schematic reconstruction chain is shown below.

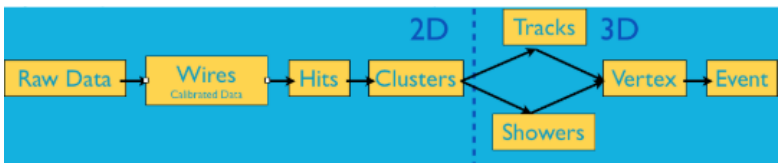

Figure 8: The reconstruction chain that LArSoft follows.[21]

Unfortunately, the data does not immediately look like the signal in figure 7. The induction planes have a bipolar signal, in which the waveform is both positive and negative. This is the effect of electrons moving towards the plane and having already passed the plane and can be observed in figure 7. With an another algorithm in the LArSoft package, the signal is deconvolved, meaning that the signal becomes unipolar, and the long-range induction effect embedded in the field response is largely removed [22]. The positively charged ions drifting with low velocities through the detector, also called space-charge, influence the electric field, which has to be corrected for. A typical example of a U-plane waveform is shown in figure 9. The measured waveform has units ADC counts. ADC stand for Analog to Digital Converter, the transformation of analog digits to a waveform. The official definition of DUNE is: "A sampling of a voltage resulting in a discrete integer count corresponding in some way to the input." For the deconvolved signal, the unit is number of electrons after scaling down by a factor 125, a factor that both ProtoDUNE as DUNE use and is experimentally determined.

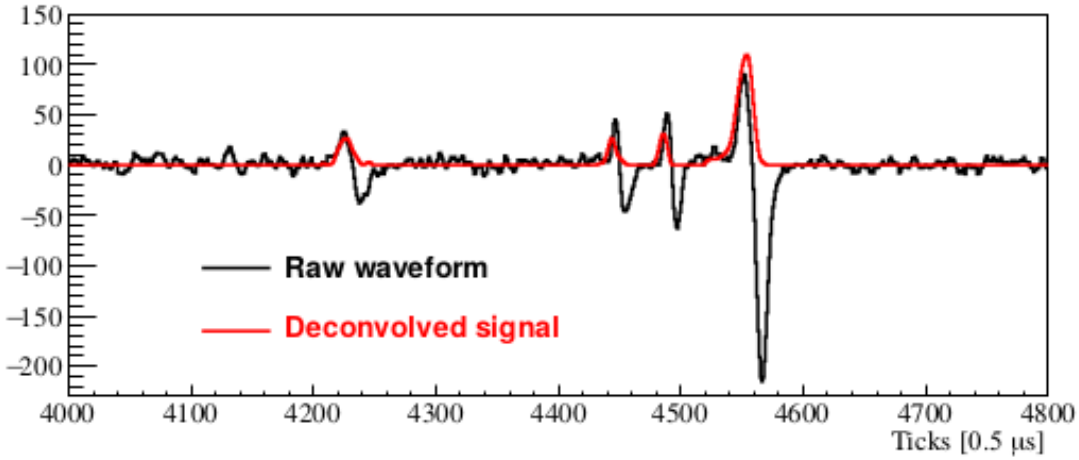

Figure 9: An example of the raw waveform from the U-plane channel of ProtoDUNE (black) and its deconvolved signal after processing (red).[22]

The steps in figure 8 are the steps the software takes to separate and label events. The events that we are interested in consist of a "cosmic" or "track", the muon, and a "shower", the Michel electron. Multiple packages are used in the code to perform the reconstruction in the following steps. First, a 2D reconstruction is needed and the first step is the calibration of raw data. The raw data are represented by objects and contain the signal output on each channel of the collection plane as a function of time. After that, the software tries to find hits. It looks for peaks in the calibrated data that indicate energy deposition. Next, the algorithm tries to identify clusters, groups of hits that belong to the same particle in both time and space. One can now start the 3D reconstruction which starts with track finding. To find a track of a muon, the software searches again for groups of hits, however this time only non-electromagnetic shower-like groups are extracted, which then get assigned a direction in three dimensions and a track length. After the finding of the muon tracks is completed, the shower-like groups, which indicate a Michel electron, must also be found. Vertex finding is the process where one searches for muon tracks and showers which come from the same origin, thus belonging together. Finally, the shower and muon track must be matched to form a single event. An event now has muon and Michel electron directions and positions. The points in space for both can be plotted into a three dimensional plot. An example of an event is shown in figure 10. Besides the track of the particles, the charge deposition of these particles is also shown. For the muon it is now clearly visible that there is a Bragg-peak where the muon loses almost all its remaining energy at once.

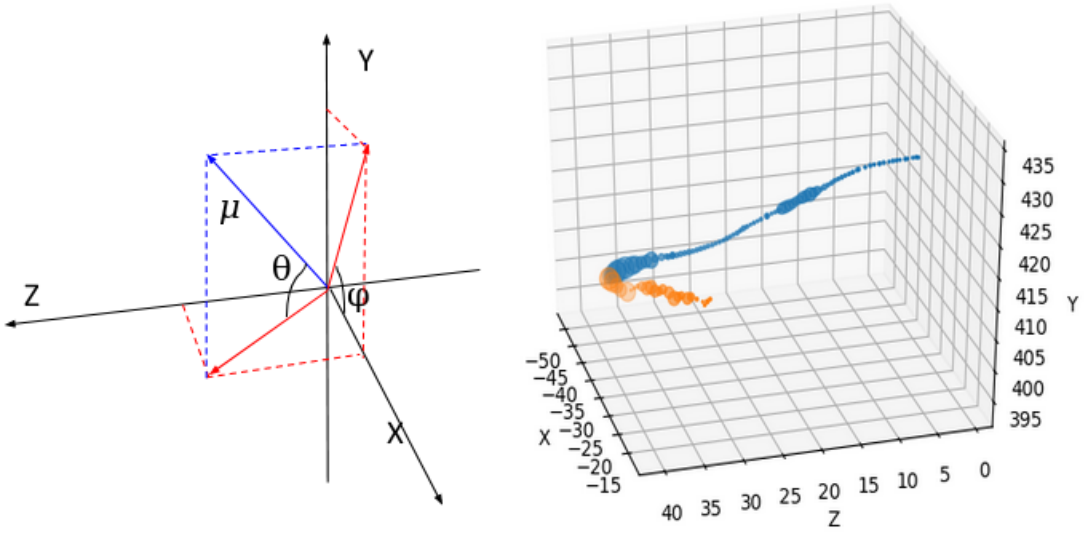

Figure 10: The right figure is created with data of ProtoDUNE by T. Miedema. The blue scatter dots represent the incident muon, the orange scatter dots represent the Michel electron. The left figure gives the spatial orientation of the detector. Where y is the vertical axis and x is the direction in which the ionized electrons will drift. The blue arrow indicates an incoming muon. The muon has an angle ϕ within the y,x-plane and an angle θ with respect to the x,z-plane. Here ϕ runs from $-\pi$ to π and θ runs from 0 to π.

The output the software generates is the total charge deposited in the wire planes through integration. The charge can be transferred into energy with the calorimetry algorithm. The electrons follow the Bethe equation quite well, however, the algorithm output of the energy loss is a three dimensional vector. This vector gives the average energy loss for a certain length along the track. With all those vectors one can integrate over the trajectory and find the total energy of the electron and muon. The data that is used in this thesis contains the charge and energy loss per unit length and well as the reconstructed kinetic energy of the electron.

Additionally, the output contains four angles: $cos(\phi_\mu)$, $cos(\phi_e)$, $cos(\theta_\mu)$ and $cos(\theta_e)$. These angles portray the momentum direction with respect to the x, y, z axes in spherical coordinates. A representation of these angles with respect to the detector plane is also shown in figure 10. One can take the inner product (equation 20) of the muon and Michel electron directions to produce the angle between the muon and the Michel electron, defined as the cosmic angle $cos(\theta)$. With this data one should theoretically be able to find the polarization of the muon through finding the best fit to the differential decay equation, because at this point it is the only unknown parameter. However, in this thesis there will be described why this is not as trivial as was thought beforehand.

$$\begin{aligned} cos(\alpha) = sin(\theta_\mu) \cdot cos(\phi_\mu) \cdot sin(\theta_e) \cdot cos(\phi_e) + cos(\theta_\mu) \cdot cos(\theta_e) \\ + sin(\theta_\mu) \cdot sin(\phi_\mu) \cdot sin(\theta_e) \cdot sin(\phi_e) \end{aligned} \tag{20}$$

4 Data analysis

Before data acquired at ProtoDUNE is used, a Monte Carlo study is held. Studying simulated data greatly helps understanding the actual data. Monte Carlo studies is a method where the user simulates the exact situation of the detector system. It includes the physics processes responsible for the interactions of the muons with the detector material, the decay of the muons and the electron trajectories in the electric field. The simulated data then follows the same steps as described in section 3.2 to find the expected values of the cosmic angle and the electron kinetic energy during the reconstruction process. Within this reconstruction process, there will also be a selection procedure where several selection cuts are made. The reconstruction process is not carried out in this thesis, only the results are used. However, in this study there will be made more selection cuts in order to analyze the data. In the following section about the simulation process, two simulations are done. The first simulation is a simulation where all muons are travelling in the same direction. After analyzing this data, it was concluded that this simulation does not cover all that is desired to see. Therefore a second simulation is done, which includes both a 1 GeV proton beam and cosmic muons from all directions, according to the cosmic spectrum. This simulation portrays the actual situation at ProtoDUNE. After explaining the simulation process, the results of both simulation processes are discussed. There is another section in between the results dedicated to the selection procedure after all the values are already reconstructed.

4.1 Simulation and selection

The idea is that muons are generated with known variables. These are the "Truth" values and will be named "true data" from this point on. The reconstruction algorithm is carried out and provides the reconstructed values. If the reconstruction algorithm is successful, the reconstructed values should match the true values. Within this reconstruction process, certain selections are made for both simulations.

The first selection is that muons end their track within the detector with a maximum of 40 cm between the muon end point and the detector bounds. Muons that pass the detector without decaying to an electron are not of interest. The second and third selections are that a muon track must be at least 90 cm long and have a minimum number of points. A point is a measure of the charge signal on the wires and there must be at least 100 of them. These are also the points that are represented in figure 10. The fourth selection is that the daughter must be shower-like. This is another way of saying that the particle originating from the muon must be shower-like, thus, an electron. The fifth selection is that the muon must be a primary particle, which is defined as the particle with which you start an event.

The last and rather controversial selection, is that there can only be one daughter of the muon. This selection is made for both the simulations. Due to bremsstrahlung, showers sometimes have more than one particle in its range. The photons that are released through bremsstrahlung can ionize argon atoms as well. They can even produce another electron via an electron-positron pair that can be considered a second daughter of the muon. The influence of bremsstrahlung on the reconstruction process is something we only discovered during this study and, unfortunately, too late to be included into the reconstruction process. The influence of bremsstrahlung on the reconstruction process based on earlier studies will still be discussed in this thesis in section 4.2.3.

These mentioned selections are all based on parameters that can be altered at any time and alterations will have an impact on the reconstruction efficiency. The simulations are done by T. Miedema who then provided the true and reconstructed data for both simulations. From this point forward, the data analysis is performed in Python version 3 with help of the pandas package[23], a package that contains the basics for data analysis. Before the data is analyzed, pandas dataframes are made, a type of storing your data. For convenience, it is desired to have alternating muon and electron rows which pair together to make an event. This results in having two dataframes. One where all the values are true data and one where all the values are the reconstructed values of the same true data. The reconstructed dataframe does have the corresponding true values in it as well, this makes the comparison between reconstructed and true data easier, which is the reason why this dataframe is used more often. The true dataframe is much larger in this case, since not all values make it through selection and reconstruction and if that happens, those events are not portrayed in the reconstructed dataframe. A lot of variables from the different dataframes are used, which makes the analysis rather complicated. In order to give more structure to this analysis, a list of variables and the corresponding dataframe is put together and shown in the appendix, section D.

The true dataframe has a label that indicates whether the reconstruction matched the truth. Reasons why the two do not match can be due to the selection cuts that are made. Additionally, the reconstructed dataframe has a label that indicates whether the reconstructed event truly contains a Michel electron. This is preferred to be the case for every particle, however sometimes the algorithm reconstructs a Michel electron where there was none. With this information two more dataframes can be made: one where the true data matches reconstruction and one where reconstruction matches the truth. These two selections of data are called the selected data. To keep all information, the unmatched events are not disposed of, but put into two more dataframes. A remark must be made here, that this is not the conventional way of selecting data, because true data is used to separate reconstructed data. When realising this method is not conventional after the first simulation, there was looked into other means of selecting the reconstructed data. This will thoroughly be described in section 4.1.2, where it will be explained why the unconventional way seems to be the only way for majority of this study. Looking at the simulations can give an insight in the functioning of the reconstruction algorithm. When the truth and reconstructed data are compared to each other, it was clear that the reconstruction is biased. There must be mentioned that the reconstruction algorithm as of now has an efficiency of ≈ 4.6 %. This value is based on what the reconstruction algorithm thinks is a Michel electron versus which event truly contains a Michel electron. Of all the events that were simulated, ≈ 25 % of the events containing a Michel electron were found. This means that a lot of simulated Michel electrons are "missed".

4.1.1 Simulation I

The first thing that was observed is that there was an enormous peak for the true data at energies around 0-0.1 MeV and for the reconstructed data there were a handful of reconstructed energies well above the energy we would suspect from theory. The cause of the peak around such low energy values are most likely to be due to δ-rays, which have been discussed earlier. In the reconstructed data this peak is lost, since it did not originate from a Michel electron, which is one of the criteria. To analyze the data through some plots, we dispose of this data, as to not warp the scale of the axes.

In figure 11 the true and reconstructed reduced energy is plotted before and after the selection of matching data. The theoretical curve that belongs to figure 11 is shown in figure 5. First, there were only negatively charged muons simulated, since it was not expected that charge

would have any influence on this study and this was simply easier. The true values have a deviation in the energy distribution when comparing this with the expected energy spectrum seen in figure 5. This can be explained as follows. In liquid argon, the energy spectrum of the Michel electron changes due to negatively charged muons being captured by the nucleus. When negatively charged muons start to come to rest, they get bound to nuclei due to their attractive Coulomb potential. The muon then falls down to the $1s$ atomic orbital. The decreasing of the energy of the bound muon slows down the decay-in-orbit (DIO) rate, but is cancelled out by the increasing of the decay probability of the electron because the electron wave function near the decay region is increasing. Even if the Coulomb interactions do not significantly modify the decay rate, they do have an influence on the electron energy spectrum.[24] This effect is also shown in figure 12. The bounding to the nuclei results in a slight shift in the peak in the spectrum and energies extending past, what we first thought was, the maximum energy all the way up to $E_e \approx m_\mu$. This also explains the handful of reconstructed energy values well past the so-called maximum energy. Another very interesting result of the bounding of muons is that due to (spin-orbit) interactions between the muon and the nucleus, they become depolarized. In bound muon decay this also results in the electron being emitted asymmetrically with respect to the muon polarization axis due to parity non-conservation.[25] This study also showed that the shift in the energy spectrum becomes larger for heavier nuclei.

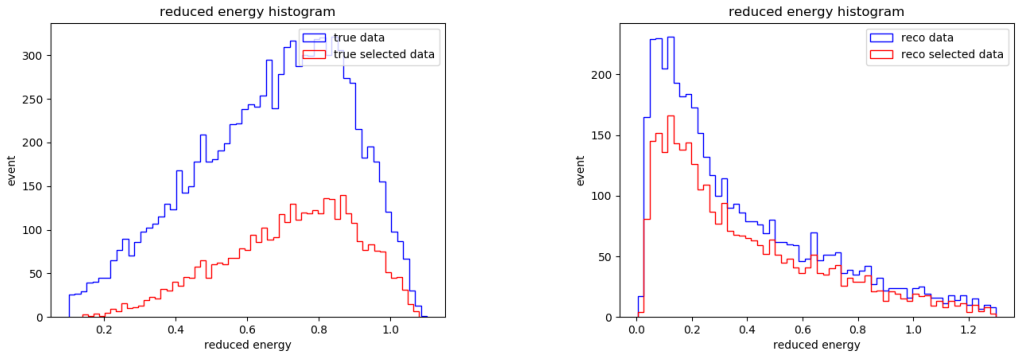

(a) (b)

Figure 11: The Michel electron energy spectrum is shown in this figure. The blue curve indicates all reduced energy values, while the red curve indicates only the values that matched after reconstruction. On the right the true values are shown, on the left the reconstructed values are shown.

The data generated in this Monte Carlo study solely used negatively charged muons, resulting in a rather large shift. For a previous ProtoDUNE study carried out by Reynolds[29], this effect was observed too. In order to check this hypothesis, the same plot should be made with data solely containing positively charged muons, which can not bound to nuclei. When the same plots are made as before, the curve for true data looks much more like expected. From a comparison of figures 11 and 13 it is clear that the capturing of negatively charged muons is indeed the cause of this effect. When looking at only positively charged muons, the steep cut-off at a reduced energy value of $x = 1$ is clearly visible. In the actual data there will be a mixture of both negatively as positively charged muons.

Now that change in the energy spectrum for true data is cleared up, there must be looked at the bigger problem. The reconstructed energy values are far too low compared to the expected curve and compared to the true values. Up until now, this is a problem that multiple people are

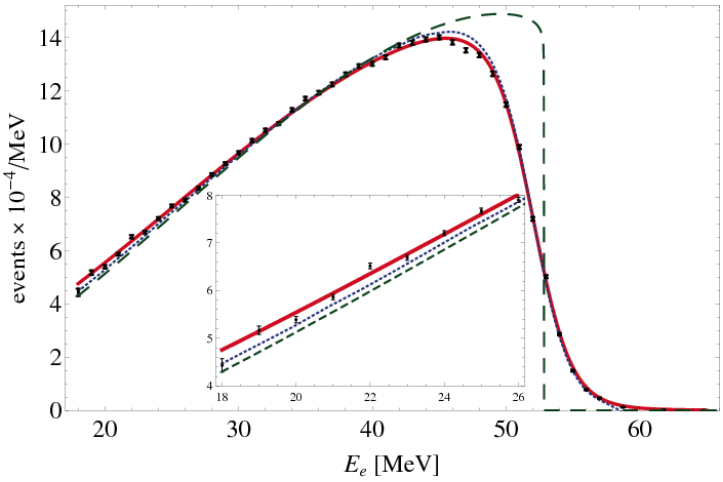

Figure 12: In this figure the influence of radiative losses on the electron energy distribution is shown. The black points resembles actual data from TWIST[26], the solid red and blue lines show the electron spectrum with and without radiative corrections of the theoretical curve up to a certain order of magnitude.[27],[28] The dashed green line shows the free muon decay electron energy spectrum with radiative corrections. This figure is enhanced with respect to the spectra that were shown before, to display the differences better.[24]

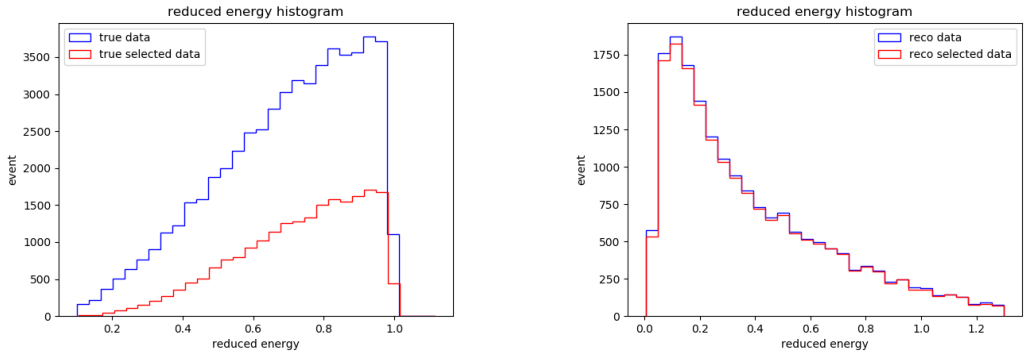

(a) (b)

Figure 13: The Michel electron energy spectrum is shown in this figure. The blue curve indicates all reduced energy values, while the red curve indicates only the values that matched after reconstruction. On the right the true values are shown, on the left the reconstructed values are shown. Only positively charged muons are considered.

working on and the main contributing factor is thought to be the influence of bremsstrahlung. However, it has also become clear that while bremsstrahlung may be the main contributing factor, it cannot be the only contributing factor. There will not be looked at bremsstrahlung due to previously mentioned reasons. This thesis does describe some other possible causes of this reconstruction problem. To put the reduced energy plots into perspective, a combined plot is made where true values are shown versus the reconstructed values. This is done with the restriction that the true and reconstructed values for a certain event must be matched and can be assured via taking data from the reconstructed dataframe including the matching true values. This two-dimensional histogram is seen in figure 14 and as is clearly visible, the reconstructed

energy values are too high with respect to their matching true values. If the reconstruction were to be successful, they ought to follow the diagonal. In this plot a mixture of both negatively and positively charged muons are used. The mixture contains $\approx 48\%$ negatively charged muons and $\approx 52\%$ positively charged muons. This ratio is more realistic when comparing this to the cosmic spectrum of the actual data. Nevertheless, it still does not represent the actual situation well enough. The second simulation, where there is both a 1 GeV proton beam and the inclusion of the cosmic spectrum, does match the situation at ProtoDUNE.

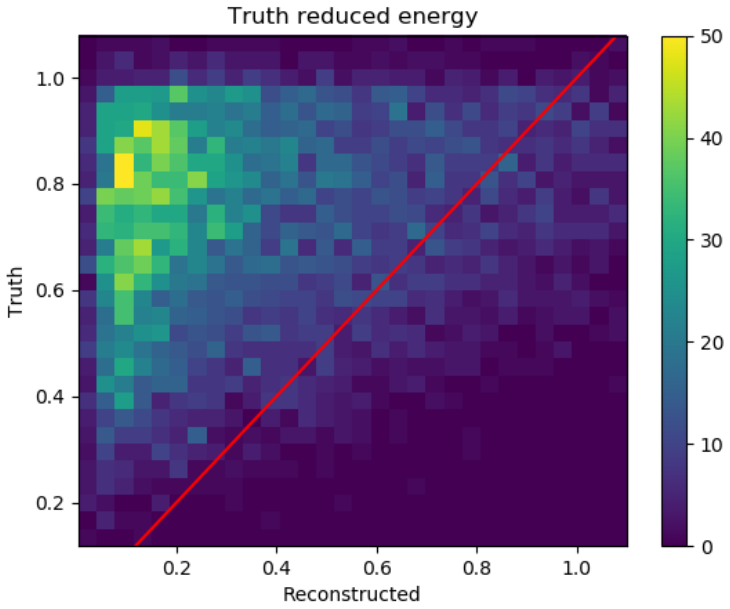

Figure 14: In this figure the reduced energy is plotted for both the true values and the reconstructed values for events that contain both components. This plot is made from data coming from only positively charged muons.

4.1.2 Selection cuts

The selection of reconstructed data in the previous section is not completely accurate. A selection of the data was made on true level. A dataframe was made for all reconstructed values where there truly was a Michel electron. Normally, a selection is based on the reconstructed values. Usually one has to find a variable, that when you plot the distribution of the variable, there is a clear indication of where to cut your data. A comparison can be made of a known distribution before and after the selection cut to see whether the selection cut was effective. In this case, the distribution of $cos(\alpha)$ was taken. From truth level, it is known what the distribution should look like. However, in the true data of the simulation, there was a relatively large peak at $cos(\alpha) \approx 1$, which did not appear in the reconstructed data. This is most likely to be caused by the reconstruction algorithm splitting a single muon track into a muon and electron track. Instead of seeing only one particle, it reconstructs two particles. Another cause could be the releasing of δ-rays, which have such low energies that they are more difficult to reconstruct. It can also be possible that the reconstruction algorithm simply matches two particles together that neither belong together nor originated near to each other in the first place. This can be checked through some new variables.

One of the new variables is the distance L between the start of the electron track and the end of the muon track. Those positions are known in three dimensions and the distance can be calculated with Pythagoras' theorem. In the detector signal, the electron track appears later in time then the end of the muon track. This is expressed in spatial difference through the reconstruction algorithm. The reconstruction algorithm then corrects for this delay. A Michel electron should therefore originate at the same point of the decay position of the muon, and L should be 0.0. The figure is enhanced for tracks between $0 - 200$ cm, the actual maximum lies around 2×10^5 cm. The distribution is so far stretched out, because there still appear to be Michel electrons originating very far from the end of the muon track This is not compatible with the true data and a cut at $L = 20$ cm can be made to rid ourselves of these values. Another variable that is used is $|\Delta E|$, where ΔE is the difference between the muon energy and the electron energy. If this distance equals zero, the tracks are coming from the same particle. Which means that the reconstruction algorithm thought a Michel electron was emitted, but in reality there was none. The true and reconstructed values overlap too much to cut in the middle. However, there seem to be a peak at small energies. Thus, the cut is made at $|\Delta E| = 120$ MeV. The third variable is the regular E_e, the kinetic energy of the electron. There seems to be an enormous peak at energies where $E_e \approx 0$. Here we must be careful, cutting the electron energy for $E_e < 1$ MeV has the risk that the electrons where the energy actually was < 1 MeV are lost too. Compared to the true values, this does not seem to be a problem. There are relatively few energies within that region.

The cuts that are made with the effect on the distribution of E_e are shown in figure 16 and 17. Those three cuts did give some improvements with respect to the cosmic angle, but not nearly enough. Figure 15 shows the distribution of the cosmic angle where only the mentioned three cuts are made and the distribution when the restriction that the reconstructed data must contain a true Michel electron. There still needed a lot of cuts to be made in order to let those two distributions match. Believing that the reconstruction algorithm is not yet the most accurate algorithm, there was chosen to select on Michel matching. A cut based on true data, but for this study, which focuses solely on Michel electrons, an accurate one. It must be remembered that this cut provides only 4.6 % of the reconstructed events. For this study, there seems to be no better solution. In figure 15 this can also be seen. The number of events is less than before. The distribution still do not exactly match, but this is most likely to be caused by the reconstruction algorithm itself, where the directions of the trajectories of the muons and electrons are not matched exactly.

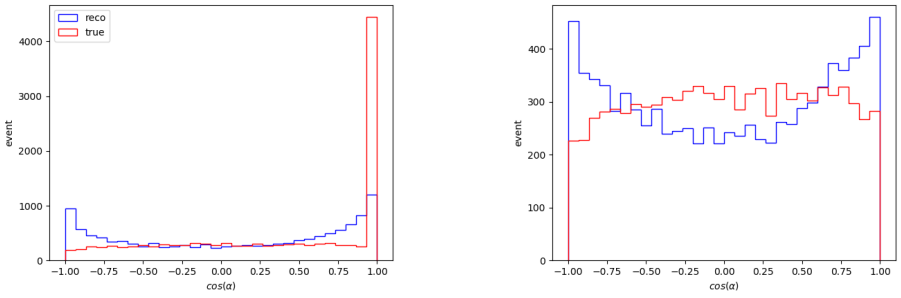

Figure 15: In this figure the distribution of the cosmic angle is shown. On the left the distribution is shown after the mentioned selection cuts, where there still appears to be a peak for cosmic angles approaching one. The right figure shows the cosmic angle distribution when there is selected on truth level. All the events that are shown contain a Michel electron.

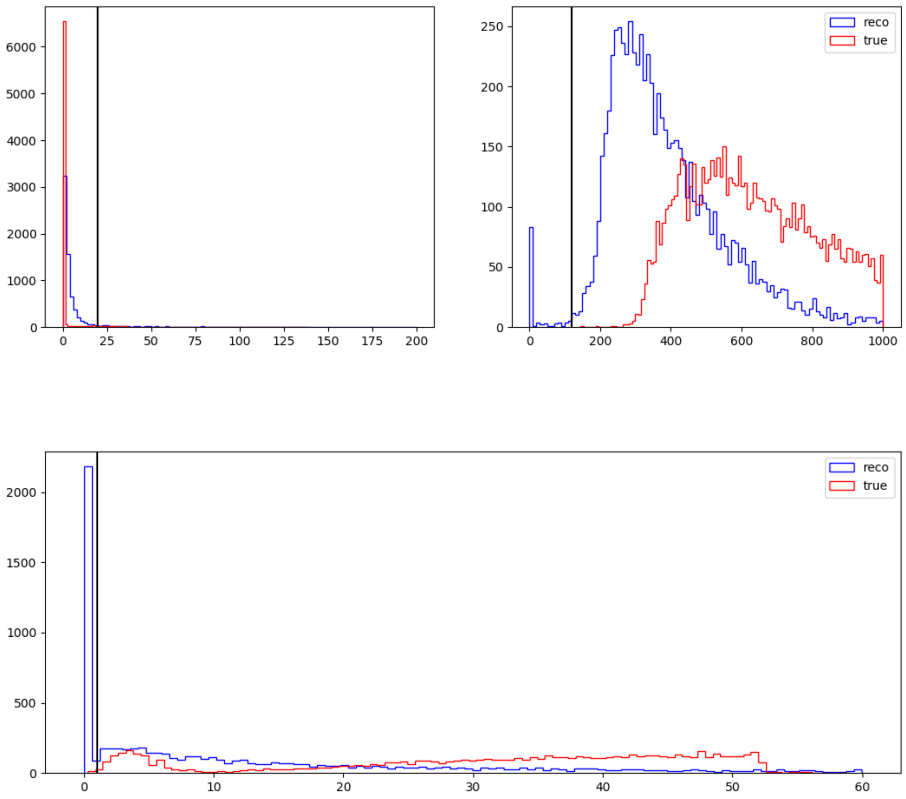

Figure 16: In this figure the distributions of respectively, L, ΔE and E_e are shown. The blue curves indicate the reconstructed values and the red curves indicate the true values. The black vertical lines show where the cut is made.

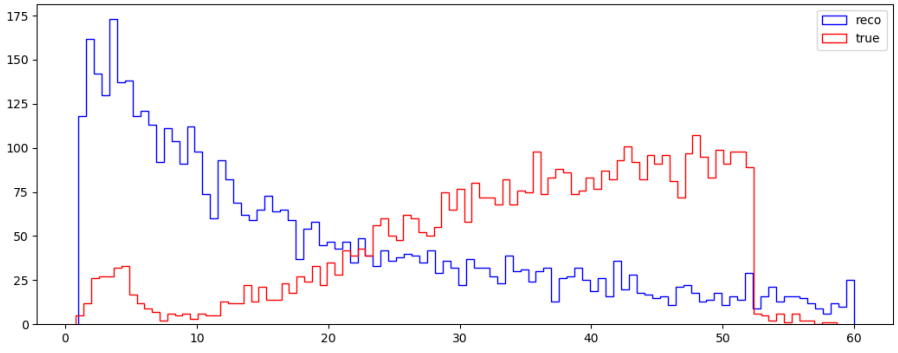

Figure 17: This is the energy distribution E_e after the cut, since it was the only non-trivial distribution out of the three compared to figure 16 it is shown a second time without the peak at $E_e \approx 0$.

4.1.3 Simulation II

The first simulation made use of muons that originated in the same direction, which means that the incident angles of the muons were fixed. To really be able to say something about the angles within the detector, a second simulation had to be performed where both a proton beam and the cosmic spectrum are included. Within the analysis of the selection cuts, the distribution of the cosmic angle from this simulation was used and can be seen in figure 15. In the beginning it was expected from the cosmic angle to have a preference for $cos(\alpha) = +1$. Although this peak was originally found in the data before making the desired selection cuts, it did not represent the actual distribution. The fact that the distribution is more spread out can be explained due to the muon ionizing many particles before decaying into a Michel electron. All those processes have an impact on the chirality and in the end it might be flattened out like we see in the plot. The mentioned peak at values approaching one, was not found in the first simulation, which means that it must be a problem that occurs when looking at cosmic muons.

Before analyzing the data more selectively through the selection cut where there is looked solely at the data where there truly was a Michel electron in the first place, a problem arose. The reconstruction software provides the two angles θ and ϕ, which were used to calculate $cos(\alpha)$. When looking at the distribution of the angles, the following distributions were found and are shown in figure 18. In this figure there were some interesting aspects. The angle ϕ is the angle of the x,y-plane, where $\phi = -\frac{1}{2}\pi$ means that that the muon is coming from directly above. This is also the position of the beam, and therefore very likely to produce muons with this angle. The cosmic spectrum that is simulated will contain muons mostly from above. This is clearly visible in the figure. The axis of angle ϕ does not stop at 0, since there are some muons coming from below the detector. This is exceptionally rare and thus not visible. The angle ϕ of the electron shows that the electrons have no preference and clearly travel in all directions of the x,y-plane. The angle θ runs from 0 to π which is expected when using spherical coordinates and defining θ as the angle with respect to the x,z-plane. It seems like there is a preference for certain values, but if the angle θ was transformed to an angle that shows the angle within the x,z-plane, it should show that all angles are represented. To make sure the right angles were used, the angles in the x,z-plane are calculated with the start and end positions of the muon track as well. This angle $\eta_{x,z}$ is defined as

$$\eta_{x,z} = tan^{-1}\left\{\frac{EndPosition_Z - StartPosition_Z}{EndPosition_X - StartPosition_X}\right\}, \tag{21}$$

where StartPosition and EndPosition are values that are provided by the reconstruction algorithm on truth level. When the angle in the x,z-plane $\eta_{x,z}$ is reconstructed with the equation above, it is clear that, indeed, all directions are represented by the cosmic muons. However, when $\eta_{x,z}$ is reconstructed with the previously known angles ϕ and θ, the distribution was not evenly spread out. Because of this fact, all angles were calculated to double-check if the orientation of the detector was understood correctly. When reconstructing ϕ, which is known to be the angle in the x,y-plane, with the same method as equation 21 uses, there was another interesting aspect that stood out. Apparently, about half of the time, the angle ϕ was off by $-\pi$. This does not have any influence on the cosmic angle $cos(\alpha)$, as long as θ shows the same effects. However, that cannot be checked in the same way.

At this point, it was unclear whether the angles provided by the algorithm were trustworthy. Especially since there is not an easy way to compare θ with the equation seen before. Therefore this simulation was run a second time, however, instead of using the software's definition of ϕ and θ, the directions are taken directly from the algorithm and only Cartesian coordinates are

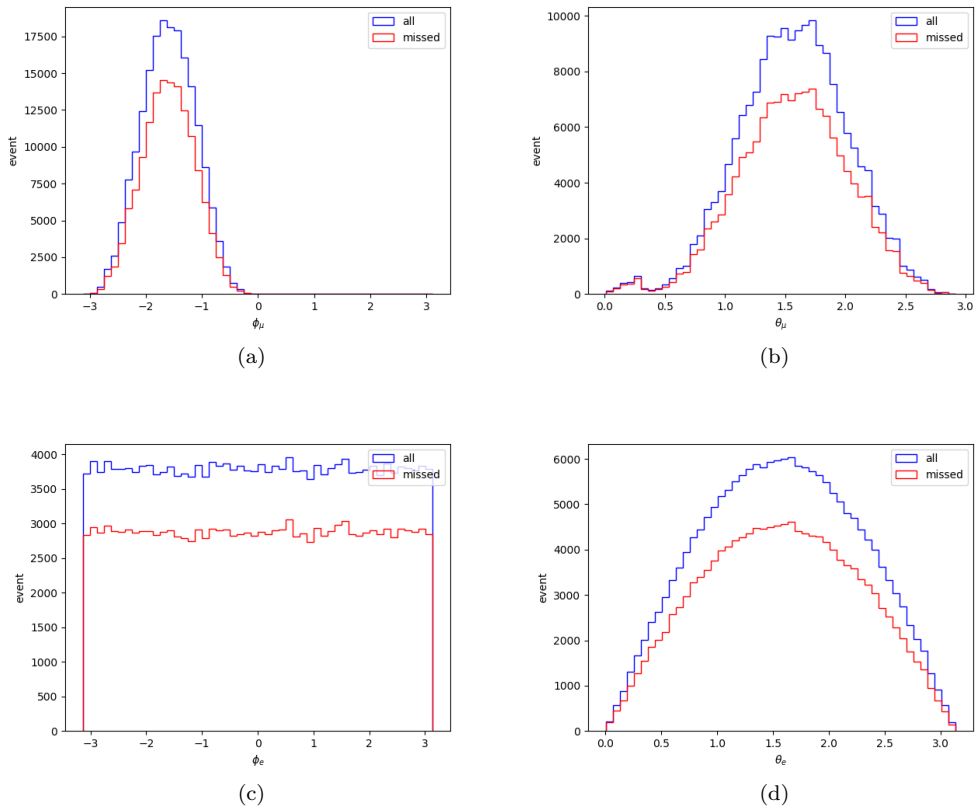

(a) (b) (c) (d)

Figure 18: In this figure the distributions of the angles ϕ and θ are shown for both the muon as the Michel electron. These plots contain only true values, where the blue curve represents all values and the red curve represents the values of the data that was not matched after reconstruction.

used to calculate the cosmic angle $cos(\alpha)$. The start and end directions of the particles are represented as normalized vectors at that particular point in the particle's track. The cosmic angle can then be found as follows.

$$cos(\alpha) = EndDirection(\mu) \cdot StartDirection(e) \tag{22}$$

The inner product of the end direction of the muon track with the start direction of the electron track will provide the cosmic angle between the two tracks. It is a much easier method and also more likely to be accurate. Luckily, the cosmic angle that was found through equation 22 did not show any major changes with the method that was used before, which indicates that the inner product of angles still provides an accurate representation. Later on, the incident angles of the particles are analyzed more closely and the new method should then provide a better analysis. Nevertheless, the cosmic angle will still be calculated with the angles θ and ϕ because the directions of the track that are used in 22 are not known on true level. Thus, the reconstruction efficiency with respect to cosmic angle distribution can only be checked with the use of the angles θ and ϕ.

4.2 Reconstruction problems

In the second simulation, there was not a significant difference for the energy distribution of the electron energy when comparing the energy spectrum with the spectrum of the first simulation. There still is a problem with the reconstruction of the electron energy. The influences of some possible causes are discussed in this section.

4.2.1 Cosmic angle

The definition of cosmic angle was discussed previously. The size of the cosmic angle can have an influence on the reconstruction process. Especially, when the cosmic angle is either $+1$ or -1. In those cases, the Michel electron will travel in the same or opposite direction of the muon track. There will not be a distinct vertex where two directions are crossing. When taking into account how the data acquisition set-up looks like, the tracks are not separated in space and time. The only way to distinguish the two will be the Bragg-peak and the fact that there might be a slight pause in induced current peaks, due to the decay process. It might be possible that the reconstruction process has more trouble distinguishing the two particles with certain cosmic angles.

In the plot of the cosmic angle, seen in figure 15, the reconstruction process matches the true values rather well, after selection. Which means that when the true and reconstructed data are plotted against each other with the restriction that every event has to be matched, the plot has a clear diagonal. This can be seen in figure 19. This indicates that the cosmic angle is reconstructed correctly. To really be able to say something about the influence of the cosmic angle, a second plot must be made.

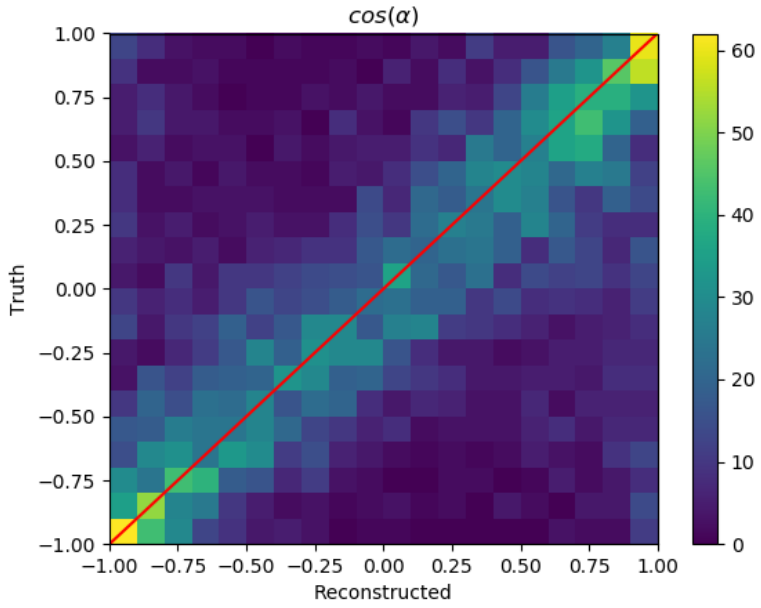

Figure 19: In this figure the true data is plotted versus the reconstructed data of the cosmic angle with the restriction that they have to be matched.

If the reconstruction process is dependent on the cosmic angle, the distribution of the cosmic angle shown in figure 19 should change if lower energy values are taken. For the optimization that was supposed to be done, there is the assumption that all variables are independent of the electron energy. To see if this assumption is correct, the same kind of plot as shown in figure 19 is made, but now for different values of the electron energy. Eight slices have been made in the data where each slice corresponds to a certain range of energy. The slices do not have to be of similar range, but contain roughly the same amount of data. If the cosmic angle is energy independent, every distribution should look like figure 19. In figure 20, there can be seen that this is roughly the case. There is some noise in the lower energy regions, but in general they look the same and the reconstruction efficiency of the cosmic angle is not energy dependent. However, the cosmic angle distribution seems to be energy dependent, where higher energies correspond to lower values of the cosmic angle. This is important if we were to perform an optimization fit, as explained in section 5.

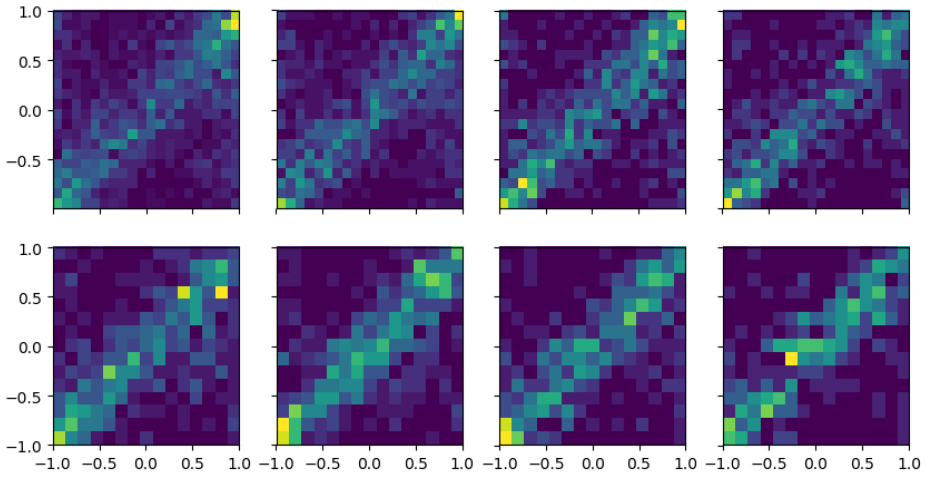

Figure 20: In this figure the true data is plotted versus the reconstructed data of the cosmic angle with the restriction that they have to be matched. This is done for eight different ranges of electron energy. The energy increases from left to right and from top to bottom.

The energy reconstruction process was already biased, seen in figure 14. The same figure can be made for values of the cosmic angle close to $+1$ and -1. If the distribution changes drastically, it is clear that the cosmic angle has an influence specifically on the energy reconstruction. When comparing figure 21 with figure 14, they seem very alike. The reconstructed energy does seem to be lower for those certain values for the cosmic angle, which means that there is a small influence of the cosmic angle on the reconstruction process. However, more data is needed to be able to put an actual percentage to this inefficiency.

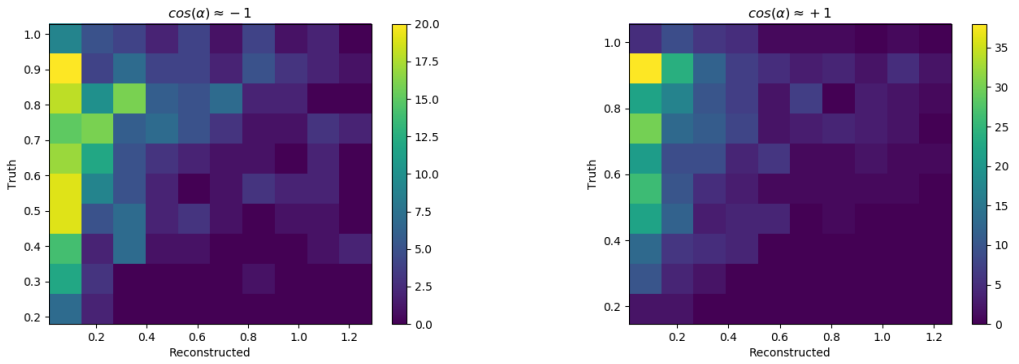

(a) (b)

Figure 21: In the figure on the left the energy values are plotted for cosmic angles smaller than -0.9. In the figure on the right the energy reconstruction efficiency is plotted for cosmic angles larger than $+0.9$.

4.2.2 Incident angle

The cosmic angle was defined by the angles ϕ and θ, the angles that indicate the direction of a particle in spherical coordinates. In the first simulation, the muons are simulated to travel in the same direction: the truth values for ϕ_μ and θ_μ are the same for every muon. In the second simulation, muons were simulated according to the real situation. After the decay of the muon, the Michel electron directions are scattered and spread out in the three dimensional plane. The importance of incident angle for this hypothesis is when the particle direction is perpendicular to the wire plane. The angles θ and ϕ were not accurate enough to analyze this. The normalized direction vectors in the three dimensional plane provide a more accurate insight. If the direction of the particle is perpendicular to the wire plane, which includes both a particle traveling towards the plane as a particle travelling away from the plane, it might be more difficult to reconstruct the energy. In figure 10 it is shown that the induced current peaks will be on different wires. However, when such a case as described above occurs, all the peaks will appear on only one wire, or a few wires at most. Distinguishing peaks, and therefore, hits from each other, could be more difficult and the reconstruction could fail. In order for this to happen the normalized direction vector of y and z should be zero while, the normalized direction vector of in the x-direction should be 1 or -1.

To check this hypothesis three plots are made. The first one being the distribution of all data, the second one being the distribution of matched data and the third one being the distribution of missed data. This is the data that did not had a successful reconstruction. Plotting the directions of the Michel electron gives an insight in why the data was not successful. After observing this data, the missing of the data is not influenced by the incident angle. Besides, the x-direction vector being ≈ 1 does not happen often enough to be able to say something about this. What does stand out are the electron direction peaks of the y and x direction being zero. This seems to have no influence on the reconstruction efficiency, but does look odd. This might be caused by Michel electrons tracks bending. When the electron direction was calculated through their start and end position, this did not seem to match with their start direction provided by the reconstruction algorithm, indicating bending of the electron track. The influence of this aspect and the relation with said peaks is not analyzed due to the absence of true values matching the reconstructed directions of the electrons.

The reconstruction of the energy for the values mentioned here is still faulty but for now there is no way of telling if this is caused by the particles travelling perpendicular to the wire planes. In the figure of the angle distribution it is also clear that the exact angles that the particle must have to travel perpendicular are not that common, especially for the incoming muon.

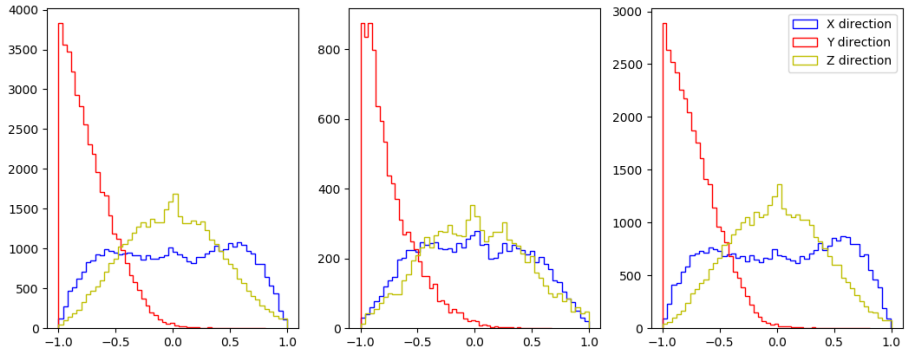

(a)

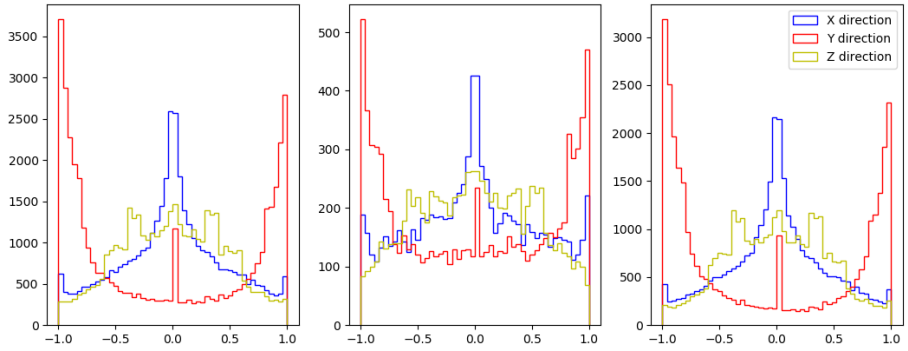

(b)

Figure 22: This figure shows the distribution of end directions of the muon (top) and the start directions of the electron (bottom). From left to right this figure shows the all data, the matched data and the missed data. Matching is defined through the previously mentioned selection cut.

4.2.3 Bremsstrahlung

The reconstruction problems could have another, more probable, cause. As was mentioned earlier, the LArSoft reconstruction algorithm uses the Bethe-formula in order to reconstruct the kinetic energy. However, the critical energy of electrons traveling through argon was 30.5 MeV and the most probable value of the electron energy from theory is about 53 MeV. The problem here is that the majority of electrons traveling though argon have a dominant energy loss in the radiative area. Meaning that radiative losses such as bremsstrahlung and pair-production are more important and dominant than ionization and excitation. If the reconstruction algorithm does not use the right formula to reconstruct the energy, it will not reconstruct it correctly for higher energetic electrons.

If bremsstrahlung happens, the produced photon could either ionize argon atoms itself or produce an electron-positron pair. The electron could then be detected too, if it loses energy trough ionization. It is important to understand that it does happen. This figure from MicroBooNE shows this rather well. MicroBooNE is a different experiment, with the same set-up. However, to check whether this is a cause of the faulty reconstruction there must be looked at the shower again. The shower was defined as only the Michel electron, but when the region of interest is expanded, the shower will also contain more detail, like in figure 23. This is done in other studies and it has become clear that this phenomenon does have an influence on the reconstruction process and must be taken into account when a correction is made.

Another method of discovering the influence on bremsstrahlung is to use the bremsstrahlung energy loss formula which is described in equation 17 instead of the Bethe-formula to reconstruct energies of the particles in the detector. If the usage of this equation provides a more accurate description of the energy distribution, it could be a clear sign of the influence of bremsstrahlung on the reconstruction process. In this equation of bremsstrahlung loss it is seen that electrons lose energy faster in radiative areas. There can be deducted that in the same amount of space, more energy is lost when looking at bremsstrahlung than if there is looked at ionization/excitation. If more energy is lost during the trajectory, the original particle has a higher energy which looks more like the theoretical approach.

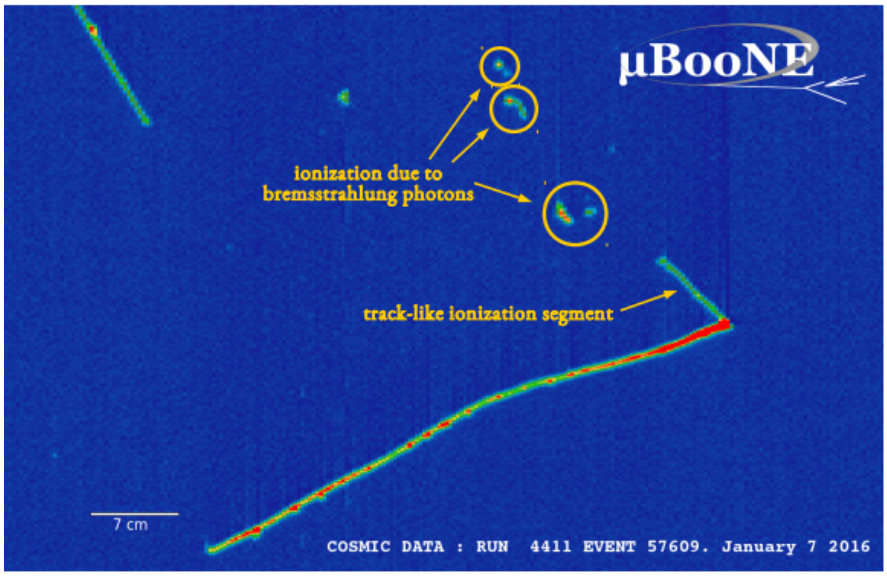

Figure 23: In this figure from μBooNE it is clear that bremsstrahlung photons are detected and play a part in the energy loss of Michel electrons.[20]

4.2.4 Bragg-peak

The final, and also very probable cause is something else to do with the reconstruction definitions. It could be very possible that the Bragg-peak of the muon does not only contain charge deposited by the muon, but also charge deposited by the electron. If the separation between the muon and electron track appears too late, the electron is not defined well. This is made harder through the reconstruction correction of the spatial separation of the tracks. The charge that is deposited quite early on in the trajectory, is not contained within its own track but taken into the Bragg-peak of the muon. The electron that is measured is then a low energetic electron.

The reason that this might be the cause is that the energy distribution behaves rather well for a low energetic electron, indicating that energy is displaced rather than lost. This is very difficult to verify.

One possibility to check this hypothesis is to look at the distribution of electron energy with respect to the cosmic angle in a two-dimensional histogram for the reconstructed data. It is expected that when the cosmic angle is either $+1$ and -1, where the two particles are moving in the same or complete opposite direction, it is more difficult to separate the two tracks. This could result in the problem discussed here happening more often. When the cosmic angle is 0 and the particles are traveling perpendicular to each other, it could be a lot easier to distinguish the two and the discussed problem should happen less often.

If the inclusion of electron energy into the muon track was indeed a cause of the faulty reconstruction, the two-dimensional histogram should show a preference for either high energetic electrons with a cosmic angle of $cos(\alpha) = 0$ and/or low energetic electrons with a cosmic angle of $cos(\alpha) = +1$ and -1. In the left figure of figure 24 it shows us the low energetic preference rather well. This indicates that besides the influence of bremsstrahlung, the definition of the Bragg-peak may have caused some reconstruction problems as well. The right figure of figure 24 is made in the first simulation, when there was looked at only positive muons coming from the same direction. The distribution is now completely different. This is either a result of the muons traveling in only one direction or the absence of the cosmic spectrum. This can only be determined when looking at actual data which is done in the next section. While keeping in mind the distribution in the left figure it should be interesting to look at the definition of the reconstruction algorithm more carefully to see if there is a problem with the distinguishing of the tracks.

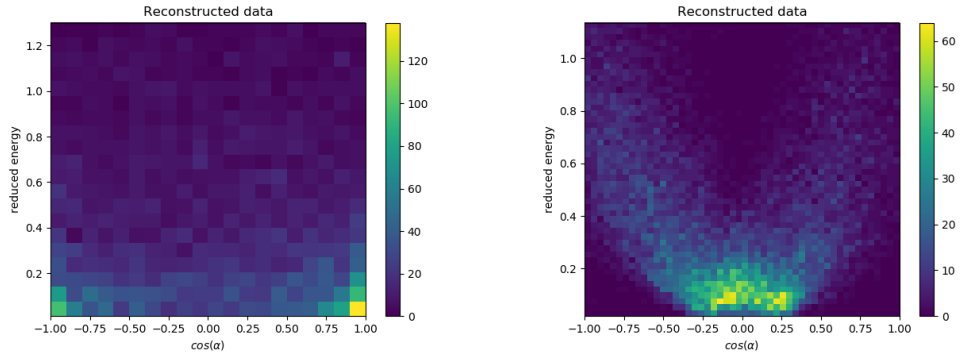

(a) (b)

Figure 24: In this figure the two-dimensional histogram of the reconstructed electron energy versus the reconstructed cosmic angle is shown. In the left figure this is done for the second simulation where muons travel in all directions. The right figure is made in the first simulation, with only positive muons coming from a fixed direction.

4.3 ProtoDUNE data

For the data that was acquired at ProtoDUNE, there are no true values. In order to analyze this data, there can only be cuts made on the reconstructed data. This is where the selection cuts from section 4.1.2 are important. When making the same cuts that are made here, the data can be compared to the figures 17 and 15. Although it is known that this does not cover the spectrum of only Michel electrons on true level, it does give an indication of the simulation and whether the simulation is accurately enough for the portrayal of actual data. The reconstruction is still biased, but if the bias is seen in both simulation and actual data, it does say something about the accuracy of the simulation itself.

The three cuts that are made are as follows. The distance L between the two tracks must be smaller than 20.0 cm. The difference in energy ΔE between the muon and the electron must be greater than 120.0 MeV. The electron energy E_e must be greater than 1.0 MeV. Two other cuts that were made here, as well as for the figures 17 and 15, to be able to compare them on the range that matters for this thesis are that ΔE must also be smaller than 1000.0 MeV and E_e must be smaller than 60.0 MeV. The results for the reduced electron energy and the cosmic angle are shown in figure 25. This figure can be compared to the figures 15 and 17. In figure 15 the left figure shows the cosmic angle distribution with the same cuts that are made here. The blue curve is the reconstructed data and when this curve is portrayed and compared to figure 25, they look quite similar. Although the cosmic angles of $+1$ and -1 seem to be more represented than in the previous curve, this is merely a result of the amount of bins that is used. Other cuts should be made to make it look exactly like the true distribution, yet these cuts are not specified. The reconstructed energy values have the same distribution as the blue curve in figure 17, which is expected.

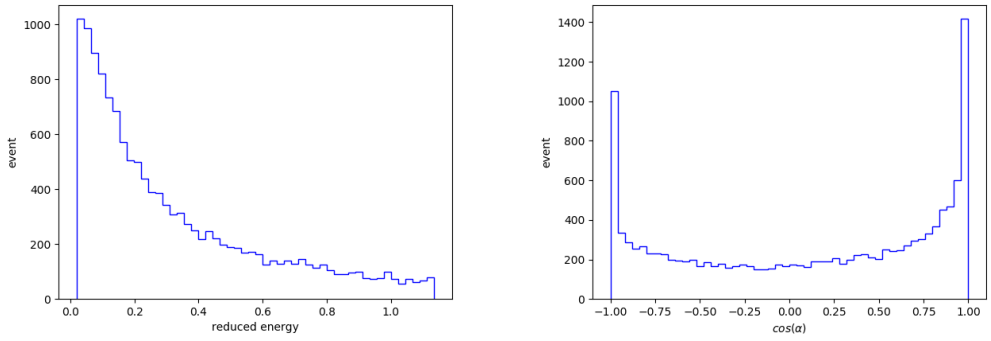

(a) (b)

Figure 25: The reconstructed energy spectrum and the reconstructed cosmic angle distribution for actual data acquired at ProtoDUNE.

In the data analysis of the Monte Carlo study, the difference in the two plots were the reconstructed energy was shown versus the cosmic angle, was clearly visible. It was not sure whether this difference arose from the fact that in one simulation the muon angles were fixed or that is was due to the cosmic spectrum. For the actual data the same figure is created and looks exactly like the figure from the second simulation. Indicating that the definition of the Bragg-peak within the reconstruction could have an influence in the reconstruction efficiency. At this point, there was another selection to be made in order to check where the difference is coming from.

In the first simulation the incident angles of the muon where fixed. Namely, $\theta_\mu = 0.2824410664$ and $\phi_\mu = -2.378425308$. Therefore, the actual data was cut for $\theta_\mu < 0.1$, $\theta_\mu > 0.35$, $\phi_\mu < -2.45$ and $\phi_\mu > -2.3$. The same figure was made to see if the incident angles have had anything to do with this difference. However, the two-dimensional histogram stayed exactly the same, but with less events. Now we know that the difference is not caused by the incident angles, it could be a cause related to the cosmic spectrum.

The last aspect that was checked, was whether the actual data have the same spectrum as the second simulation that was carried out. To really remove the relation with incident angles, the incident angles have to be similar to the second simulation. In figure 26 this seems to be exactly the case when comparing this figure with figure 22. The same angles are equally represented for the muon. For the electron there still seems to be the spikes at 0 for both the x- and y-directions. The origin of those peaks is not yet cleared up.

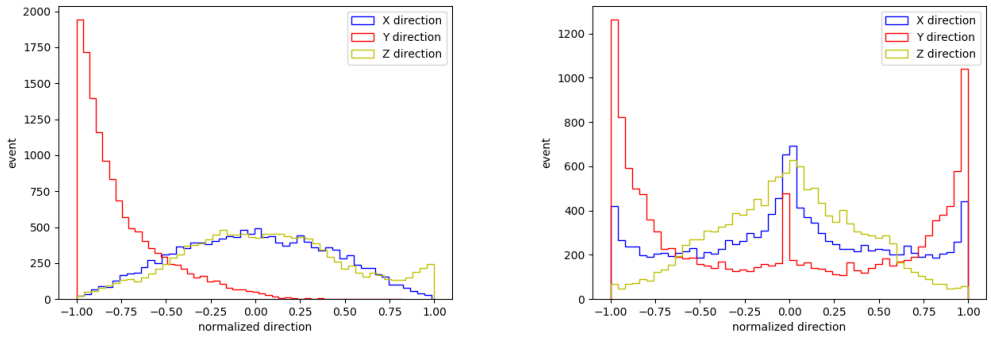

(a) (b)

Figure 26: The distributions of the directions of, respectively, the muon and the electron in three dimensions.

5 Conclusion and discussion

In this thesis, the correction on the theoretical curve is mentioned more than once. The main goal of this thesis was to find the polarization via fitting the data to the theoretical curve. However, it became clear that the reconstructed data did not look like the theoretical curve at all. A fit would therefore not obtain the right results. In order to carry out the fit, the theoretical curve should be corrected. Before any correction factor could be found, the cause of the faulty reconstruction should be found. This is where the second problem arose. There was not a known single cause for this faulty reconstruction, although there are some very probable ideas.

In this thesis we tried to shine some light into the causes of the reconstruction problem. While bremsstrahlung has been speculated about longer, I wanted to look into other possible causes as well. There were some hypothesis that seemed to have an influence, but how big or how important their influence is, is not determined. Therefore, if a correction must be made, all those causes should be taken into consideration without a known weighing factor or the correction factor they provide. This is hardly doable, especially for a thesis this size and with an unknown parameter (P_μ). Instead, the reconstruction problems were elaborated on more, where it became clear that besides bremsstrahlung there might also be an influence resulting from the definition of the Bragg-peak reconstruction where part of the charge deposited by the electron is included into the muon track. A comparison with the real data that was obtained at ProtoDUNE has also been made. In this comparison we were able to remove some speculations as well as proving the existence of problems within the reconstruction process. The fact that the actual data resembles the simulation so well, is a step forward in the right direction. While there are still many problems with the reconstruction process, the actual data does not show any unexpected distributions with respect to this reconstruction process.

In a future study there are many possibilities. If I were to continue in this subject, the correction would be a first step. To have one equation, including every correction term with a certain correction factor, to be able to fit the data to, would be a great start. It does, however, avoid the most pressing question. Why is this reconstruction biased and where in the reconstruction process does this go wrong? There is probably something in the reconstruction algorithm that is not taking into account one or more of the reconstruction problems that are discussed in this thesis. If this could be helped, a correction would not be necessary in the first place but a greater understanding of the reconstruction algorithm would be.

The last thing that I want to remark is that when, in the end, the data follows a theoretical curve, where either the theoretical curve is corrected or the reconstruction is corrected, a polarization fit can be made. Since this was the original idea for this thesis, I was able to describe this process, which can be done with two methods. The "least square method" and the "most likelihood estimation" are both legitimate methods to find the best fit to the curve. For both cases we look at equation 6. Both methods use the expected fraction of events per bin $f_i(P)$, which is the only term dependent on the parameter P. The expression for $f_i(P)$ is given in equation 30 in appendix A.

In the least square method a sum is made over all the squares of the differences between expected values and measured values. The squares are scaled with the statistical error ϵ_i squared. The sum is minimized to find the parameters that show the least amount of deviation of the expected values from the measured values. The least square equation is defined as

$$s^2 = \sum_{i=1}^{N_{bins}} \frac{(n_i - f_i(P))^2}{\epsilon_i^2}, \tag{23}$$

where N_{bins} is the number of bins, n_i is the fraction of measured events per bin compared to the total number of events, $f_i(P)$ is the expected fraction of events per bin compared to the total expected number of events, and ϵ_i is the statistical error per bin. ϵ_i can also be described as the standard deviation of the binomial distribution which depends on f_i and N, the total number of events, as follows.

$$\epsilon_i = \sqrt{\frac{f_i(1-f_i)}{N}} \tag{24}$$

If s^2 described the least square method well enough it should follow a χ^2 function[30] and through optimization, the unknown parameter can be deducted.

The most likelihood estimation uses a rather different method. Normally, one would look at $f_i^{n_i}$ and find the maximum of the likelihood L. In Python, the command *scipy.optimize* is used. This looks at the minimum of an equation. Because of this, it is easier to look at the logarithms of the likelihood estimation. It is trivial that for the maximum of L, the maximum of $\log(L)$ is located at the same position. Since the command looks at a minimum, not a maximum, a simple minus sign is put in front. The other positive result of taking the logarithm is the fact that n_i is now not a power, but can be put in front of the logarithm, reducing the computing capacity that is needed to perform this calculation. The final likelihood function is therefore defined as

$$\log(L) = -\sum_{i=1}^{N_{bins}} (n_i \log(f_i(P)), \tag{25}$$

where N_{bins} is the number of bins, n_i is the fraction of measured events per bin compared to the total number of events and $f_i(P)$ is the expected fraction of events per bin compared to the total expected number of events.

The polarization of the muon was believed to be ± 1 from a theoretical approach. During the process of carrying out this study, a lot was learned about the interaction with matter as well as data analysis. The hypothesis about the polarization was altered during the writing of this thesis. In the theoretical approach, the interactions with argon atoms was not included. While traveling through argon, the muon bounces off thousands of argon atoms. All these interactions have an influence on the polarization and the polarization could be "flattened out". Or in other words, approach zero. For the true data of the Monte Carlo study, which followed the theoretical curve well, the polarization fit was carried out. Indeed, these values of P tend to be closer than 0. To be able to really say something about this polarization change of muons losing their energy in liquid argon, the polarization fit must be made with the actual data, which cannot be done while the reconstruction is biased. Nevertheless, I am of opinion that the interactions of high energetic cosmic muons with argon atoms will have an influence on the polarization. On how big this influence really is, only a following study can provide answer.

A Integration of differential decay

A.1 Total integration

The differential decay width is a differential equation depending on $cos(\alpha)$, the angle between the muon and the electron, the reduced energy $x = \frac{2E_e}{m_\mu}$ and the polarization of the muon P_μ. Integrating this equation over $cos(\alpha)$ rids us of P_μ and makes it only energy dependant. This is needed for the selection procedure.

$$\begin{aligned} \frac{\partial^2\Gamma}{\partial x \partial cos(\alpha)} &= \frac{G_F^2 m_\mu^5}{192\pi^3}(3 - 2x \pm P_\mu cos(\alpha)(2x-1))x^2 \\ \frac{\partial\Gamma}{\partial x} &= \frac{G_F^2 m_\mu^5}{192\pi^3}(3cos(\alpha) - 2xcos(\alpha) \pm P_\mu \frac{1}{2}cos^2(\alpha)(2x-1))x^2 \end{aligned} \tag{26}$$

$cos(\alpha)$ runs from -1 to 1. When these boundaries are filled into the equation we obtain:

$$\frac{\partial\Gamma}{\partial x} = \frac{G_F^2 m_\mu^5}{192\pi^3}(6x^2 - 4x^3) \tag{27}$$

This equation gives us the energy distribution of the electron. If this equation is integrated over x we retrieve:

$$\Gamma = \frac{G_F^2 m_\mu^5}{192\pi^3}(2x^3 - x^4) \tag{28}$$

x runs from 0 to 1. Where 1 means that E_e has reached its maximum value. This results in:

$$\Gamma = \frac{G_F^2 m_\mu^5}{192\pi^3} \tag{29}$$

This is exactly the value we should obtain, since it equals the inverse of the muon lifetime.

A.2 Integration per bin

For a two dimensional histogram a single bin i has boundaries for $cos(\alpha)$: $\{c_{1,i}, c_{2,i}\}$ and the reduced energy x: $\{x_{1,i}, x_{2,i}\}$. To integrate over these boundaries the expected value of decays per bin is found. Dividing this value by the total decay integration(29), the fractional expected value $f_i(P_\mu)$ is found.

$$\begin{aligned} f_i(\{c_{1,i}, c_{2,i}, x_{1,i}, x_{2,i}\}; P_\mu) =& \{c_{2,i}x_{2,i}^3 - \frac{1}{2}x_{2,i}^4 c_{2,i} \pm P_\mu c_{2,i}^2[\frac{1}{2}x_{2,i}^4 - \frac{1}{3}x_{2,i}^3] \\ &- \{c_{1,i}x_{2,i}^3 - \frac{1}{2}x_{2,i}^4 c_{1,i} \pm P_\mu c_{1,i}^2[\frac{1}{2}x_{2,i}^4 - \frac{1}{3}x_{2,i}^3] \\ &- \{c_{2,i}x_{1,i}^3 - \frac{1}{2}x_{1,i}^4 c_{2,i} \pm P_\mu c_{2,i}^2[\frac{1}{2}x_{1,i}^4 - \frac{1}{3}x_{1,i}^3] \\ &+ \{c_{1,i}x_{1,i}^3 - \frac{1}{2}x_{1,i}^4 c_{1,i} \pm P_\mu c_{1,i}^2[\frac{1}{2}x_{1,i}^4 - \frac{1}{3}x_{1,i}^3]\} \end{aligned} \tag{30}$$

B Physical constants

Symbol	Definition	value
$m_e c^2$	electron mass $\times c^2$	$(0.510\,998\,946\,1 \pm 0.000\,000\,003\,1)$ MeV
$m_\mu c^2$	muon mass $\times c^2$	$(105.658\,374\,5 \pm 0.000\,002\,4)$ MeV
c	speed of light	$2.997\,924\,58 \times 10^{-8}\,\mathrm{m\,s^{-1}}$
$\hbar$	Plank's constant	$1.054\,571\,8 \times 10^{-34}\,\mathrm{m^2\,kg\,s^{-1}}$
G_F	Fermi coupling constant	$(1.166\,378\,8 \pm 0.000\,000\,7) \times 10^{-5}\,\mathrm{GeV^{-2}}$
α	fine structure constant	$1/137.035999173$
α_w	fine structure constant weak interaction	$\approx 1/29.5$
r_e	classical electron radius	$(2.817\,940\,322\,7 \pm 0.000\,000\,001\,9)$ fm
K	$4\pi N_A r_e^2 m_e c^2$	$0.307\,075\,\mathrm{MeV\,mol^{-1}\,cm^2}$

C Definitions

Symbol	Definition	
v	velocity	βc
γ	Lorentz factor	$\frac{1}{\sqrt{1-\beta^2}}$

D Dataframe layout

	Dataframe i		Dataframe ii	
	Reconstructed	True	True	Used for
Energy	cosmicKineticEnergy	TruthP	TruthP	x, ΔE
Position	cosmicStartPosition[0]	TruthStartPosition[0]	TruthStartPosition[0]	η, L
	cosmicStartPosition[1]	TruthStartPosition[1]	TruthStartPosition[1]	
	cosmicStartPosition[2]	TruthStartPosition[2]	TruthStartPosition[2]	
	cosmicEndPosition[0]	TruthEndPosition[0]	TruthEndPosition[0]	
	cosmicEndPosition[1]	TruthEndPosition[1]	TruthEndPosition[1]	
	cosmicEndPosition[2]	TruthEndPosition[2]	TruthEndPosition[2]	
Direction	cosmicStartDirection[0]			$cos(\alpha)$
	cosmicStartDirection[1]			
	cosmicStartDirection[2]			
	cosmicEndDirection[0]			
	cosmicEndDirection[1]			
	cosmicEndDirection[2]			
ϕ	cosmicPhi	TruthPhi	TruthPhi	$cos(\alpha)$
θ	cosmicTheta	TruthTheta	TruthTheta	
Match	cosmicTrueMichel	RecoMatched	RecoMatched	Selection

E Figures

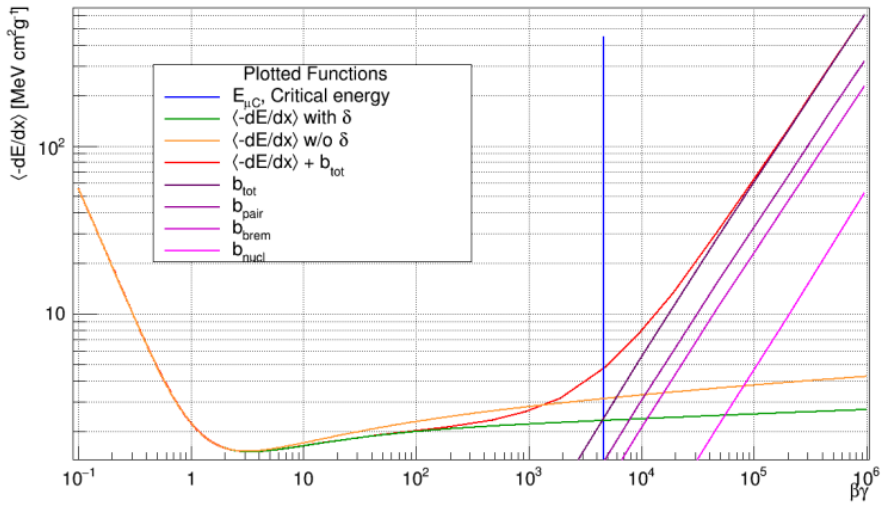

Figure 27: The energy loss of a muon in liquid argon with and without the density correction. Here, contributions of other means of energy loss are also taken into account.[15]

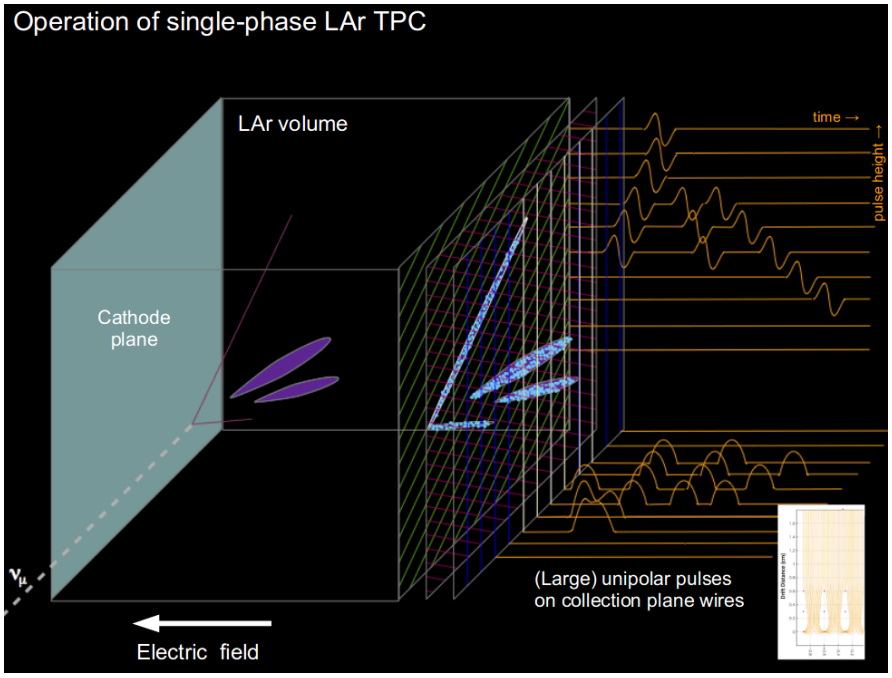

Figure 28: A muon neutrino entering the LArTPC and the corresponding induced signals which overlap.[31]

References

[1] CECCHINI S, SIOLI M. Cosmic Ray Muon Physics. 1998;p. 18. Available from: https://arxiv.org/abs/hep-ex/0002052.

[2] Clay R, Dawson B. Cosmic Bullets, High Energy Particles in Astrophysics; 1997.

[3] Thomson M. Particle Physics: Handout 9 : The Weak Interaction and V-A. 2009;Available from: https://www.hep.phy.cam.ac.uk/~thomson/lectures/partIIIparticles/Handout9_2009.pdf.

[4] Meredith L. Helicity, chirality, and the Dirac equation in thenon-relativistic limit. 2018;Available from: https://www.pas.rochester.edu/assets/pdf/undergraduate/helicity_chirality_and_the_dirac_equation_in_the_non-relativistic_limit.pdf.

[5] Gerosa R, Marzocchi B, Mastrolorenzo L. Measurement of Life-Time and P-Violation in Polarized Muon Decay. 2011;.

[6] Turner R, *et al* . Polarization of Cosmic Ray Muons. Phys Rev D. 1971;4(1). Available from: https://journals.aps.org/prd/abstract/10.1103/PhysRevD.4.17.

[7] Dobbs A. *Muon Ionization Cooling Experiment (MICE)*. Imperial College London;. Available from: https://wwwf.imperial.ac.uk/blog/mice/2017/09/01/introducing-mice/.

[8] Tanabashi, *et al* . REVIEW OF PARTICLE PHYSICS: Muon Decay Parameters. Physical review. 2018;98(3):617–620. Available from: https://journals.aps.org/prd/pdf/10.1103/PhysRevD.98.030001.

[9] Hörandel J. Particles and the Cosmos lecture 1: Interactions with matter. Radboud University. 2019;Available from: http://particle.astro.ru.nl/goto.html?partcos1920.

[10] Jones B. INTRODUCTION TO SCINTILLATION LIGHT INLIQUID ARGON;Available from: https://microboone-exp.fnal.gov/public/talks/LArTPCWorkshopScintLight_bjpjone_2014.pdf.

[11] *Liquid Argon Properties (Tables and Calculators)*. LAr @BNL;. Available from: https://lar.bnl.gov/properties/.

[12] Grupen C, Shwartz B. Particle Detectors. 2nd ed. Cambridge University Press; 2008.

[13] Tanabashi, *et al* . REVIEW OF PARTICLE PHYSICS: Particles Through Matter. Physical review. 2018;98(3):446–461. Available from: https://journals.aps.org/prd/pdf/10.1103/PhysRevD.98.030001.

[14] Sternheimer RM. The Density Effect for the Ionization Loss in Various Materials. American Physical Society, Phys Rev. 1952 11;851(88). Available from: https://doi.org/10.1103/PhysRev.88.851.

[15] Ingles K, Junk T, Marchionni A. Muon Energy Loss in Liquid Argon. Fermilab;Available from: https://indico.fnal.gov/event/14933/contribution/10/material/paper/0.pdf.

[16] Bichsel H. Straggling in thin silicon detectors. Rev Mod Phys. 1998;663(60). Available from: https://journals.aps.org/rmp/pdf/10.1103/RevModPhys.60.663.

[17] Landau L. On the energy loss of fast particles by ionization. J Exp Phys. 1944;201(8):201–205. Available from: http://inspirehep.net/record/45074/.

[18] *An International Experiment for Neutrino Science*. Deep Underground Neutrino Experiment;. Available from: https://www.dunescience.org/.

[19] Abi B, *et al* . The Single-Phase ProtoDUNE Technical Design Report. 2017 02;Available from: http://inspirehep.net/record/1606328?ln=en.

[20] Acciarri R, *et al* . Michel Electron Reconstruction Using Cosmic-Ray Data from the MicroBooNE LArTPC. JINST. 2017;12(9). Available from: http://inspirehep.net/record/1590896?ln=en.

[21] *LArSoft Reconstruction Chain*. LArSoft Wiki;. Available from: https://cdcvs.fnal.gov/redmine/projects/larsoft/wiki/Reconstruction.

[22] Deep Underground Neutrino Experiment (DUNE) Technical Design Report. 2019 10;2. Available from: https://dune.bnl.gov/docs/dune-tdr/vol-physics.pdf.

[23] *Python Data Analysis Library*. NumFocus;. Available from: https://pandas.pydata.org/.

[24] Czarnecki A, Dowling M, Garcia i Tormo X, Marciano WJ, Szafron R. Michel decay spectrum for a muon bound to a nucleus. Phys Rev. 2014;D90(9):093002.

[25] Watanabe R, Fukui M, Ohtsubo H, Morita M. Angular Distribution of Electrons in Bound Muon Decay. Prog Theor Phys. 1987;78:114–122.

[26] Grossheim A, Bayes R, Bueno JF, Depommier P, Faszer W, Fujiwara MC, et al. Decay of negative muons bound in ^{27}Al. Phys Rev D. 2009 Sep;80:052012. Available from: https://link.aps.org/doi/10.1103/PhysRevD.80.052012.

[27] Watanabe R, *et* , *al* . At. Data and Nucl. Data Tables. 1993;54(165).

[28] Czarnecki A, Tormo X, Marciano W. Muon decay in orbit spectra for muon-electron conversion experiments. 2011 11;.

[29] Reynolds A. Michel Electron Reconstruction. 2017;Available from: https://indico.fnal.gov/event/15181/session/6/contribution/38/material/slides/0.pdf.

[30] Cochran WG. The χ^2 Test of Goodness of Fit. Ann Math Statist. 1952 09;23(3):315–345. Available from: https://doi.org/10.1214/aoms/1177729380.

[31] Snider E. *Intriduction to LArSoft*. Fermilab;. Available from: https://indico.fnal.gov/event/9928/session/8/material/2/0.